CHAPTER 1

Fuel Processing for Fuel Cells

Torsten Kaltschmitt[1] and **Olaf Deutschmann**[2,3,*]

Contents

[1] Institute for Nuclear and Energy Technologies, Karlsruhe Institute of Technology (KIT), Karlsruhe, Germany
[2] Institute for Catalysis Research and Technology, Karlsruhe Institute of Technology (KIT), Karlsruhe, Germany
[3] Institute for Chemical Technology and Polymer Chemistry, Karlsruhe Institute of Technology (KIT), Karlsruhe, Germany
* Corresponding author. E-mail: deutschmann@kit.edu

Advances in Chemical Engineering, Volume 41
ISSN 0065-2377, DOI: 10.1016/B978-0-12-386874-9.00001-4

Abstract This chapter focuses on processing the different fuels for the use in fuel cells, that is, the chemical conversion of different hydrocarbon fuels to hydrogen or hydrogen-rich synthesis gases. Aside from an overview on fuels, fuel processors, and fuel requirements from the perspective of different fuel cells, quantitative modeling and simulation approaches are presented. The models are based on the molecular chemical processes in heterogeneous fuel conversion and describe the interactions of chemical reactions on catalytic surfaces and in the gaseous fluid with mass and heat transport. Reforming of natural gas, gasoline, diesel, and ethanol are discussed.

ABBREVIATIONS

AC	alternating current
APU	auxiliary power unit
ATR	autothermal reforming
AUVs	autonomous undersea vehicles
BGBI	Federal Law Gazette
BOP	balance of plant
C/O	carbon-to-oxygen ratio

CHP	combined heat and power
CPOX	catalytic partial oxidation
CPU	central processor unit
D	dimension
DC	direct current
DFT	density functional theory
DIN	German Industry Standard
DMFC	direct methanol fuel cell
DR	dry reforming
E10	gasoline blended with 10 vol.% ethanol
E5	gasoline blended with 5 vol.% ethanol
E85	gasoline blended with 85 vol.% ethanol
EG	European Community
EN	European Standard
EPA	Environmental Protection Agency
Eq	equation
EU	European Union
FAME	fatty acid methyl ester
HDS	hydrodesulfurization process
HTS	high-temperature stage in WGS
ISO	International Organization for Standardization
LLNL	Lawrence Livermore National Laboratory
LNG	liquefied natural gas
LPG	liquefied petroleum gas
LTS	low-temperature stage in WGS
MCFC	molten carbonate fuel cell
MEA	membrane electrode assembly
MF	mean-field approximation
PAFC	phosphoric acid fuel cell
PAHs	polyaromatic hydrocarbons
PEM	proton exchange membrane
PEMFC	proton exchange membrane fuel cell
POX	partial oxidation
PrOX	preferential oxidation of carbon monoxide
R&D	research and development
S/C	steam-to-carbon ratio
SMET	selective methanation of carbon monoxide
SOFC	solid oxide fuel cell
SR	steam reforming
UBI-QEP	unity bond index–quadratic exponential potential method
WGS	water–gas shift

LIST OF UNITS AND SYMBOLS

%cal	caloric percentage
°C	degree celsius
kg	kilogram
kJ	kilojoule
kW	kilowatt
m	meter
mg	milligram
mm	millimeter
mm^2	square millimeter
MW	megawatt
mW	milliwatt
n	number of moles
ppm	parts per million
ppmv	parts per million by volume
ppmw	parts per million by weight
pS	pico-Siemens
vol.%	volume percentage
W	watt
A_i	name of species i
A_k	pre-exponential factor, mol, m, s
C(s)	surface carbon
c_i	species concentration, mol m^{-2}, mol m^{-3}
E_{a_k}	activation energy, J mol^{-1}
$F_{cat/geo}$	ratio of the total active catalytic surface area in relation to the geometric surface area of the fluid–solid interphase
$\overrightarrow{j}_i$	diffusion flux of species i, kg m^{-2} s^{-1}
k_{f_k}	rate coefficient of the forward reaction, mol, m, s
K_s	number of surface reactions
M_i	molar mass of species i, kg mol^{-1}
$\overrightarrow{n}$	(surface) normal
N_b	bulk species absorbed by the catalyst particle
N_g	species in the gas phase
N_s	species adsorbed on the top catalyst layer
R	gas constant, J K^{-1} kg^{-1}
R_i^{het}	local chemical source term species i
$\dot{s}_i$	molar net production rate of species i, mol m^{-2} s^{-1}
t	time, s
T	temperature, K
Y_i	mass fraction of species i
β_k	temperature exponent

Γ	site density, mol m^{-2}
ΔH^0_{298}	molar standard formation enthalpy, J mol^{-1}
ε_{i_k}	coverage-dependent activation energy parameter, J mol^{-1}
η	effectiveness factor based on the Thiele modulus
Θ_i	surface coverage of species i
μ_{i_k}	coverage-dependent reaction order parameter
ν'_{ik}	stoichiometric coefficient
ν''_{ik}	stoichiometric coefficient
$\overrightarrow{v}_{\text{Stef}}$	Stefan velocity, m s^{-1}
ρ	density, kg m^{-3}
σ_i	coordination number, gives the number of surface sites which are covered by the adsorbed species

1. INTRODUCTION

The first successful ascension of a balloon filled with hydrogen on December 1st, 1783, in Paris was possible, thanks to prior intensive fuel processing, because Jacques Charles was eventually able to sufficiently clean the hydrogen he gathered from the dissolution of metal in acid. In their experiments in the years before, Goethe, Lichtenberg, and Soemmering in Göttingen and Frankfurt also observed the hydrogen bubbles but failed to realize their dreams of filling a balloon with them due to insufficient fuel processing (Sandstede, 2000).

In this book, fuel processing is understood as the process in which the chemical composition of chemical energy carriers (primary fuels) is chemically converted to a composition with which a fuel cell can be operated. As hydrogen is the most commonly used fuel for fuel cells, fuel processing usually is the conversion of the primary fuel to hydrogen or hydrogen-rich gases and removal of components such as sulfur and carbon monoxide that may have hazardous effects on the fuel cell operation. Since a variety of primary fuels is of interest, and since there is a variety of fuel cell types with very different requirements regarding the fuel quality, various concepts of fuel processing have been developed, depending not only on the primary fuel and the fuel cell type, but also on the field of application and its operating and boundary conditions.

Today, the lack of an adequate infrastructure for hydrogen distribution requires the delivery of hydrogen stored in bottles and tanks to the location of the fuel cell. This hydrogen is mainly produced from natural gas by large-scale industrial steam reformers associated with the need of an extensive input of external energy and a tremendous output of the greenhouse gas carbon dioxide. Therefore, from a sustainable point of view, little is gained by using fuel cells for the production of electrical

power, unless the entire process chain, from the fuel source to the produced electricity, is more efficient than the conventional production of electricity in power plants. Here, the advantages of using fuel cells for power supply include local independence from the power grid (mobile and portable applications) and their use as back-up systems in case of a grid power outage or shortage.

Due to the problems in hydrogen delivery infrastructure and since efficient hydrogen storage facilities are still under development, an alternate way of providing hydrogen for the fuel cell is the on-site production from logistic fuels. Regenerative and liquid fossil fuels exhibit a much higher volumetric energy density, which makes on-site production of hydrogen an even more attractive possibility, in particular for portable and mobile applications. On-site production requires efficient, compact, and low-cost fuel processors specifically designed for the application under consideration. A survey of current and potential fuel cell applications is shown in Table 1, which also shows the large range of electrical power output needed from the fuel cell stack, ranging from milliwatts to megawatts.

Though the topic ''fuel processing'' includes a variety of objectives, ranging from the development of sulfur-resistant reforming catalysts to the control of the entire fuel processor/fuel cell system, this chapter focuses on the physicochemical fundamentals and the engineering aspects of fuel processors specifically designed for fuel cell applications; books such as the one by Kolb (2008) and specific literature are frequently referenced for more details. Figure 1 provides a flowchart of fuel processing from the original feedstock (natural gas, crude oil, coal, biomass) to the electrochemical oxidation of the fuel cell's fuel hydrogen. Here in this chapter, the focus is on the specific fuel processing in reformers to prepare the fuel for its use in fuel cells.

The chapter is organized as follows: In Section 2, the requirements on fuel quality are given from the fuel cell point of view. Section 3 provides a short overview of all the fuels considered as source for processing for fuel cell applications. Then, there are three different sections on fuel processing being (Section 4.1) the cleaning and pre-reforming of the primary fuel (desulfurization, cracking of long-chain hydrocarbons), (Section 4.2) conversion of primary hydrocarbon fuels into hydrogen or hydrogen-rich synthesis gases, and (Section 4.3) the cleaning and composition optimization of the products such as removal of CO and olefins. In Section 4.2, we discuss all relevant hydrocarbon conversion processes, which are steam reforming (SR), partial oxidation (POX), and autothermal reforming (ATR) from the point of view of the primary fuels being natural gas, methanol, ethanol, gasoline, and diesel. Section 5 presents current available technologies and devices on the market and under construction and

Table 1 Application areas of fuel cell systems and their characteristics

Application	Purpose	Power output	Fuel cell type	Primary fuels	Fuel processor	Technology status
Power plant	Grid supply	100 kW to 500 MW	SOFC MCFC	Natural gas, coal	SR, internal reforming	Commercially available (e.g., DFC®, PureCell®)
Stationary	Electrical power	10–50 kW	SOFC MCFC	Hydrogen, natural gas, biofuels, MeOH	(H_2 tank) SR, ATR, internal reforming	Commercially available (e.g., DFC®, PureCell®)
Residential	Electrical power and heat (CHP systems)	500 W to 5 kW	SOFC PEMFC	Natural gas, biogas, LPG	Mostly ATR	Commercially available (e.g., BlueGen®)
Mobile—drive train	Electrical power	10–500 kW	MCFC PEMFC	Hydrogen, diesel	(H_2 tank) mainly ATR	Under development
Mobile—APU	Electrical power, heat supply	1–5 kW	SOFC PEMFC	Hydrogen, diesel, kerosene	SR, ATR	Under construction/development
Portable	Electrical power	1–150 W	DMFC PEMFC	MeOH, hydrogen	Internal reforming (H_2 storage)	Under development

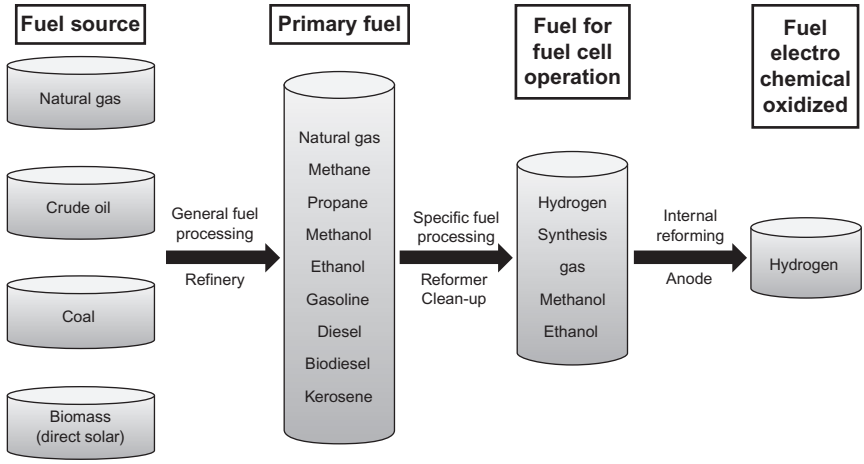

Figure 1 Chart of fuel flow from source to power; this chapter focuses on specific fuel processing (processing step 2), including some notes on internal reforming (processing step 3); the latter one is also covered in the chapter by Kee *et al*.

in development. Section 6 presents modeling approaches and Section 7 applies them to study different aspects of fuel process technologies.

2. REQUIREMENTS ON FUEL QUALITY

Table 2 summarizes common types of fuel cells regarding operating temperature and electrode materials. Since the proton exchange membrane (PEM) fuel cell has the strongest requirement on the quality of the fuel and is the most common cell so far, it should be discussed in more detail.

The PEM fuel cell is operated with hydrogen and oxygen/air at temperatures between 60 °C and 120 °C. The membrane electrode assembly of the proton exchange membrane fuel cell (PEMFC) is composed of a proton-conducting membrane and two electrodes that contain a catalyst—usually platinum—to dissociate and oxidize the hydrogen on the anode side and reduce the oxygen on the cathode side upon diffusion of the hydrogen protons through the membrane.

The conventional PEMFC anode is sensitive to carbon monoxide because CO is preferentially adsorbed on the Pt catalyst, which inhibits the hydrogen adsorption and hence poisons the anode. CO poisoning is reduced with increasing temperature because the adsorption–desorption equilibrium is slightly shifted toward desorption. Furthermore, platinum alloys may partially suppress CO poisoning by offering a route toward CO_2 formation by adsorbed water. A certain amount of air (''bleed air'')

Table 2 Type of fuel cells

	SOFC	MCFC	PEMFC	PAFC	DMFC
Operating temperature	600–1000 °C	~650 °C	60–120 °C (HT-PEM up to 170–180 °C)	190–200 °C	25–90 °C
Electrolyte	Yttria-stabilized ZrO_2	Li_2CO_3 K_2CO_3	Nafion (polybenzimidazole)	H_3PO_4	Nafion
Anode material	Ni–ZrO_2	90% Ni, 10% Cr	Pt Pt/C	Pt/C	Pt Pt/C
Cathode material	Sr-doped $LaMnO_3$	Li-doped NiO	Pt Pt/C	Pt alloy/C	Pt Pt/C
Anode reaction	$H_2 + O^{2-} \rightarrow H_2O + 2e^-$	$H_2 + CO_3^{2-} \rightarrow H_2O + CO_2 + 2e^-$	$H_2 \rightarrow 2H^+ + 2e^-$	$H_2 \rightarrow 2H^+ + 2e^-$	$CH_3OH + H_2O \rightarrow CO_2 + 6H^+ + 6e^-$
Cathode reaction	$O_2 + 4e^- \rightarrow 2O^{2-}$	$O_2 + 2CO_2 + 4e^- \rightarrow 2CO_3^{2-}$	$O_2 + 4H^+ + 4e^- \rightarrow 2H_2O$	$O_2 + 4H^+ + 4e^- \rightarrow 2H_2O$	$3/2O_2 + 6H^+ + 6e^- \rightarrow 3H_2O$

added to the fuel channel also preferentially oxidizes CO. The CO tolerance level currently ranges from <10 ppm for Pt-based anode materials up to about 100 ppm for CO tolerant anodes (Oetjen *et al.*, 1996).

Quite a number of further species in the fuel cell feed, originating either from the primary fuel or formed in the fuel processing system, can be hazardous to the PEMFC anodes. At concentrations above 250 ppm, formaldehyde and formic acids can lead to irreversible damage. Ammonia and sulfur, in particular hydrogen sulfide, have severe poisoning effects. Detrimental effects can also result in the presence of very small amounts of metallic components in the feed, which may originate from the fuel processor catalyst and material.

PEMFCs are usually rather tolerant concerning methane (up to 5 vol.%) and methanol (up to 0.5 vol.%) content in the feed.

An alternative to the classical Nafion membrane is polybenzimidazole doped with phosphoric acid, which can be operated at temperatures up to 170 °C. This material does not require humidification and is CO tolerable up to 1 vol.%.

3. PRIMARY FUELS

Since the term *fuel* is used in many different contexts in fuel cell research and development (R&D), we use the term primary fuel for the fuel that is the feedstock of the fuel processer, in which this primary fuel is converted to a fuel that can be used by a fuel cell. Today, all commercially available primary fuels are based on hydrocarbon fuels, mainly from fossil fuels (natural gas, oil, coal) but meanwhile also from biomass. Furthermore, hydrogen is the standard fuel for fuel cells, although some (higher-temperature) cells can be operated with other fuels as well. Consequently, processing of the primary fuel is needed. Another consequence is that any statement of fuel cell efficiency has also to account for the upfront fuel processing costs (energy/exergy, CO_2 emissions).

Table 3 provides a list of primary fuels available on the market. Of all current potential primary fuels, the largest volumetric and specific (per kg) amount of hydrogen (energy) is carried in liquid hydrocarbons.

3.1 Hydrogen as a primary fuel

Hydrogen as a primary fuel is not relevant today but may play a significant role in the near future as soon as efficient and inexpensive technologies become available to provide the energy for the production of hydrogen by (direct) solar energy via photovoltaic, photocatalysis, and by solar-thermo devices and (indirect) solar energy via biomass.

Table 3 Physical properties of primary fuels used for fuel processing for fuel cells

Fuel	Molecular weight [g/mol]	Density (15 °C) [kg/m^3]	Boiling point [°C]	Autoignition temperature [°C]	Flash point [°C]	Heat of vaporization [kJ/mol]	Heat capacity (C_p) [J/(mol K)]	LHV [kJ/mol]	HHV [kJ/mol]	Sulfur content [ppmw]
Hydrogen	2.02	0.084	−252.76	560	<−253	0.91	29	242.3	286.5	0
Methane	16.04	0.671	−161.5	595	−130	8.17	34.92	802.3	889.3	0
Propane	44.1	1.91	−42.1	540	−104	19.04	73.6	2011	2220.8	0
Methanol (liquid)	32.04	790	64.6	470	11	35.21	79.5	638.1	726.1	0
Ethanol (liquid)	46.07	789.4	78	425	12	38.56	112.4	1329.8	1368	0
								[kJ/kg]	[kJ/kg]	
Natural gas	16.0–20.0	0.66–0.81	−162	540–580	−188			47,141	52,225	0.25
LPG		510–580	−42 to 0	494	−104			46,607	50,152	–
Gasoline	113	720–775	50–200	280	−43			43,500	46,500	10
Kerosene	170	750–845	150–325	210	38			43,100	46,200	<3000
Diesel	202	820–845	160–371	260	>52			42,612	45,575	10–50
Biodiesel (FAME)	292	860–900	315–350	177	>130			37,520	40,160	<10

3.2 Fuels from coal

Coal, as a fossil fuel, has a very low hydrogen/carbon atomic ratio and is burned in most cases to generate energy, for example, in power plants. The gasification of coal leads to a syngas containing hydrogen, which is mainly burned in gas turbines to produce electricity.

$$C + H_2O \rightarrow CO + H_2, \quad \Delta H^0_{298} = +131\,\mathrm{kJ\,mol^{-1}} \tag{1}$$

(Throughout this chapter, all reaction enthalpies are given for gaseous species exclusively.) The produced syngas can be used in fuel cell applications after gas clean-up process steps such as desulfurization and carbon monoxide removal. These units can be quite costly depending on the coal used. Brown coal, for example, has a sulfur content of up to 3 vol.%. Therefore, coal is usually not used for fuel cell applications unless it is available at a low price. Furthermore, the produced syngas can be used for the synthesis of other fuel types, for example, methanol, ethanol, and Fischer–Tropsch fuels.

3.3 Fuels from crude oil

The actual composition of fuels derived from crude oil widely depends on its oil source and its processing in the refinery. The composition may have severe impacts on the fuel processor, in particular concerning coking issues. As most fuels are a mixture of a few up to several hundreds of hydrocarbons, for example, gasoline or diesel fuel, they are commonly classified according to their physical properties, such as boiling range, flash point, viscosity, and heating value. Their production process determines these physical properties, which are gained by blending different refinery fractions to obtain the desired values. Since today's fuels are specially tailored for internal combustion engines, fuel processors have to handle them as commercially available products, regardless of any chemical properties of the fuel that would result in a more effective reforming and hydrogen production.

In both crude oil and natural gas-derived fuels, the sulfur content is crucial for the fuel processor, in particular for the activity of the catalysts used. The sulfur content in the fuel is determined by the sulfur removal in the refineries, and the amount of sulfur left in the fuel is eventually determined by legislative regulations.

3.3.1 Liquefied petroleum gas

Liquefied petroleum gas (LPG) is a mixture of certain specific hydrocarbons which stay at room temperature and moderate pressure in the liquid phase. Main constituents are hydrocarbons with three or four carbon atoms derived from refinery processes, natural gas processing, and in

smaller amounts from cracking processes of higher hydrocarbons. The most common commercialized products for LPG are mixtures of propane and butane, which exhibit the highest specific hydrogen content among fossil fuels and, taking the weight of the hydrogen storage tank into account, could even exceed that of liquefied hydrogen (Muradov, 2003).

3.3.2 Gasoline

Gasoline is a middle distillate fraction of crude oil blended with several other hydrocarbon and polymer compounds. Originally, gasoline was a waste product of the refinery process used for producing kerosene from petroleum. Due to its high combustion energy, it became the preferred automobile fuel. Today's gasoline production is performed in a three-step process at the refinery. First, crude oil is distillated and separated in different fractions by boiling ranges. In a second step, refinement of these fractions by means of cracking, branching/isomerization, and aromatizing is performed. In the last step, unwanted contents, such as sulfur, are removed. Therefore, gasoline is a mixture of several hundreds of hydrocarbons, alkanes, including cycloalkanes, alkenes, and aromatics (Table 4), and has a boiling range from 50 °C to 200 °C. Commercial gasoline is a blend of different refinery fractions, which meets specified physical properties required for modern internal combustion engines. These specifications (e.g., EN 228 in Europe allows up to 5 vol.% bioethanol in gasoline) are regulated by the legislative authorities. Furthermore, additional additives are solved in the gasoline fuel. These additives are organic compounds that enhance certain performance characteristics or provide characteristics not inherent in the gasoline. Typically, additives are added in the ppm concentration range. Additives in commercial gasoline are antioxidants, corrosion inhibitors, demulsifiers, dyes and markers, anti-icing agents, and drag reducers. Most of them are organic alcohols or acids, polymers, soluble

Table 4 Typical composition of liquid products of petroleum (biodiesel for comparison)

	Gasoline	Diesel	Kerosene	JP-Fuel (JP-4 exemplary)	Biodiesel
n-Paraffins	4–7	40–70	10.13	32	
i-Paraffins	25–40		60.37	31	
Aromatics	20–50	<30	18.68	21	
Naphthalenes/olefins	6–16	10–30	0.03	16	
FAME	0	<7	0	0	>96
Typical chain length	C4–C12	C8–C25	C10–C16	C4–C16	C12–C22

solids, or aromatic amines. The chemical complexity of commercial gasoline fuel covers a wide field of organic compounds, all of which contribute to the reforming behavior in fuel processors. It was shown that, for example, linear alkanes have nearly the same reforming performance independent from the chain length, while branched or aromatic hydrocarbons behave completely different (Hartmann *et al.*, 2009a). There is still a high demand for catalyst research regarding the management of the reforming process of a broad variety of hydrocarbon compounds, the toleration of certain amounts of sulfur in the fuel, and the avoidance of coke formation on the catalytic surface.

3.3.3 Diesel

Diesel fuels, just as gasoline fuels, are a distillate fraction of crude oil and were originally straight-run products. The production of diesel fuel is analogous to that of gasoline: first distillation, second various conversion steps, and third clean-up. Diesel fuel contains more nonvolatile components than gasoline (Table 4) and has a higher boiling range (lying between 160 °C and 371 °C). Therefore, diesel fuel must be sprayed and cannot be evaporated in air without risking pre-ignition. Like gasoline, diesel fuel is mixed with several additives to adjust performance characteristics. Unlike gasoline, however, there are two main issues regarding additives in diesel fuel. The first is keeping the injector nozzle clean and the second is preventing gelling in cold weather when temperature falls below a certain point.

Since diesel fuel has a broad variety of characteristics, several definitions and various classifications are used in different countries, for example, DIN EN 590 in Europe. Since 2009, ultra-low sulfur diesel may only contain 10 ppm sulfur in Europe, whereas, in the USA, road diesel may contain up to 15 ppm. Since 2010, diesel fuel may contain up to 7 vol.% fatty acid methyl ester (FAME) in Europe to meet biofuels directives.

3.3.4 Kerosene

Like diesel, kerosene is an originally straight-run fraction of petroleum. Its boiling range varies between 150 °C and 350 °C and its volatility lies between those of gasoline and diesel fuel. In general, kerosene is used as jet fuel and as fuel for domestic burners and furnaces. The chemical composition of kerosene differs from that of gasoline and diesel fuel. Kerosene must be free of aromatic and unsaturated hydrocarbons, as well as of sulfur compounds. It is mostly a mixture of saturated hydrocarbons ranging from C_{10} to C_{16} in chain length. Therefore, kerosene is not produced by a cracking process. Kerosene typically consists of *n*-alkanes, alkyl benzenes, and naphthalenes.

3.4 Fuels from natural gas

Even though the methane content in natural gas may vary between 70% and 96%, the remaining hydrocarbons, mainly ethane, propane, and butane, have only minor effects on the fuel processor performance. In both crude oil and natural gas-derived fuels, the sulfur content is crucial for the fuel processor, in particular for the activity of the catalysts used. For most applications in fuel cell operation, the natural gas has to be converted into syngas in a fuel processor, providing a hydrogen-rich fuel gas for the fuel cell stack. Furthermore, the produced syngas can be processed into other hydrocarbon compounds, such as alcohols or Fischer–Tropsch fuels.

3.4.1 Propane

There are two technologies for recovering propane from natural gas, either cryogenic separation or adsorption plants. The former includes simple refrigeration which typically operates at $-23\,^{\circ}C$ for dew point control operations or at $-40\,^{\circ}C$ for propane recovery. Turbo-expander systems are well established for propane recovery. When operated at temperatures down to $-73\,^{\circ}C$, most of the ethane and all C_{3+} hydrocarbons are liquefied and afterward fractionally distilled for components separation. Figure 2 shows a typical natural gas processing diagram.

3.4.2 Methanol

Methanol can be produced by a variety of different processes. The most frequently used industrial process is the formation of methanol from syngas of Cu/ZnO- or CuO/ZnO-based catalysts, mainly supported on Al_2O_3 (Liu *et al.*, 2003; Phan *et al.*, 2011). The synthesis is carried out at moderate temperatures of about 250–300 °C at pressures of 50–100 bars and is a moderately exothermic reaction.

$$CO + 2H_2 \rightarrow CH_3OH, \quad \Delta H^0_{298} = -91\,kJ\,mol^{-1} \tag{2}$$

$$CO_2 + 3H_2 \rightarrow CH_3OH + H_2O, \quad \Delta H^0_{298} = -49.5\,kJ\,mol^{-1} \tag{3}$$

$$CO + H_2O \rightarrow CO_2 + H_2, \quad \Delta H^0_{298} = -41.2\,kJ\,mol^{-1} \tag{4}$$

In the first two reactions, (2) and (3), methanol is produced under thermodynamic control at low temperatures to avoid hot spots in the reactor. In parallel, water–gas shift (WGS) reaction consumes the produced water in reaction (3), resulting in a strong overall driving force of the reaction to the product side. Methanol is particularly used as a transportation fuel or as a convenient means of energy storage for fuel cell

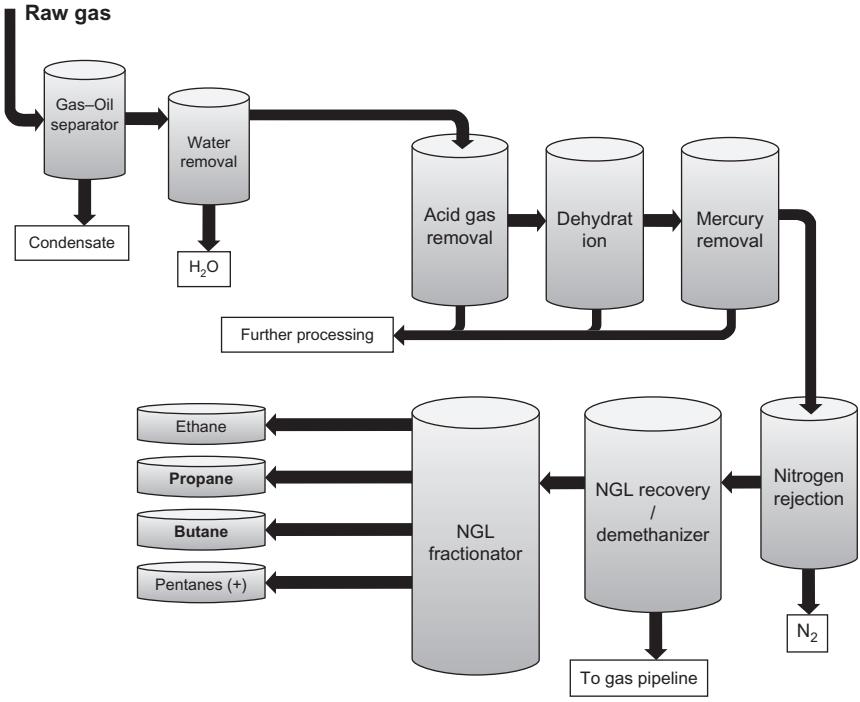

Figure 2 Simplified block flow diagram of a typical gas processing plant.

applications. Direct methanol fuel cell (DMFC) can be directly fueled with methanol without any upstream fuel processor for hydrogen production.

3.4.3 Ethanol

Ethanol and higher alcohols have been identified as potential additives for fuel in fuel cell applications. The production of alcohols $C_{>1}$ is often obtained by the catalytic conversion of syngas, which can derive from several carbon sources, such as biomass, coal, or natural gas. Rhodium-based catalysts give high selectivities to C_{2+} oxygenates, but are quite costly. Cupper-based catalysts promoted with alkali, transition metals and their oxides, and rare earth oxides are under current research as substituents for the expensive precious metal catalysts. An optimal amount of promoter with well-defined reaction conditions is necessary to suppress undesired by-products, for example, methane (Gupta *et al.*, 2011). Apart from Rh- and Cu-based catalysts, modified Fischer–Tropsch and Mo-based catalysts can be used (Spivey and Egbebi, 2007). Ethanol improves the octane rating of gasoline and reduces emissions of NO_x and unburned

hydrocarbons (Courty *et al.*, 1990), but also diminishes the overall energy efficiency. Ethanol can also be produced from biomass and is therefore of interest as biofuel due to limited fossil fuel resources.

3.5 Fuels from biomass

3.5.1 Biodiesel

The characteristics of biodiesel regarding the use in an internal combustion engine make it a fuel equivalent to diesel fuel made from petroleum. Biodiesel is made from biological sources by means of esterification of vegetable oils with methanol or ethanol; the most common sources are soybeans and rapeseeds.

The main chemical components of biodiesel are fatty acid alkyl esters. It has clean burning properties, virtually no sulfur content, and is a good lubricant. Therefore, biodiesel is blended with diesel fuel derived from petroleum. In the European Union (EU), up to 7% biodiesel can be added to ultra-low sulfur diesel from the refinery since 2010. When it comes to boiling range, viscosity, and specific density, the physical characteristics of biodiesel are comparable to diesel fuel.

In Europe, the EN 14214 standard determines the minimal requirement for biodiesel fuel, for example, maximum 10 ppm sulfur content.

3.5.2 Ethanol

Ethanol derived from biomass, which is also referred to as bioethanol, is produced from the conversion of carbon-based feed stocks, such as sugar-based (sugar cane, sugar beets), starch-based (corn, grain), and cellulose-based (straw, wood) raw material.

The increasing use of renewable fuels, for example, ethanol, and fossil fuels blended with renewable fuels, for example, E10 (gasoline blended with 10 vol.% ethanol), in vehicles also intensifies the research activities for these fuels in the field of hydrogen supply (Hohn and Lin, 2009; Nilsson *et al.*, 2008).

3.5.3 Methanol

Methanol was historically produced by gasification of organic materials followed by methanol synthesis, or by destructive distillation of wood. However, the obtained methanol was of lower quality and contained additional contaminations such as halide ions. Today, methanol is mainly produced by the conversion of synthesis gas in the presence of cupper-based catalysts at moderate temperatures of about 250 °C. The synthesis gas can either be derived from natural gas or from biomass gasification. Depending on the source, additional clean-up and adjustment steps have to be implemented in the process to produce high-quality methanol.

In the EU, there are directives for the usage of energy derived from renewable resources, which regulate the share of renewable energy in the overall energy demand of the EU's member states by 2020. In consequence of 2009/28/EG, Germany introduced the BioKraftQuG in 2006. BT-Drs 16/2709 regulates the percentage of biofuels in vehicle fuels. In 2009, it was revised by BGBl. I S. 1804. For gasoline, a caloric percentage (%cal) of 2.8%cal, and for biodiesel 4.4%cal is dictated.

4. FUEL PROCESSING TECHNOLOGIES FOR FUEL CELL APPLICATIONS

Converting hydrocarbon fuels to a hydrogen-rich syngas including fuel preprocessing and reformate clean-up is a complex chemical and engineering task. Various processor steps are integrated in a fuel processing system according to the used primary fuel or the requirements on the reformat quality. In the following, the main steps as preprocessing of the fuel, reforming, and clean-up are discussed. The main focus is given to the conversion of hydrocarbon fuels to hydrogen. A full fuel processing system is shown in Figure 3.

4.1 Cleaning of the primary fuel—Desulfurization, pre-reforming/cracking of large hydrocarbons

Fuel sources, such as natural gas, crude oil, coal gas, and especially biomass, contain significant amounts of sulfur. For reformer and fuel cell usage, desulfurization is necessary. As a consequence of strict directives by the EU and Environmental Protection Agency, USA regarding the reduction of sulfur dioxide emissions, the maximum allowed sulfur levels in these fuels need to be reduced. Figure 4 shows the maximum allowed sulfur content for different fuels over the past 20 years. In 2010, sulfur levels were limited to 10 mg kg^{-1} in the EU (Euro V) and to 15 mg kg^{-1} in the USA.

A conventional method for desulfurization treatment of fuel at the refinery is the hydrodesulfurization process which is operated at 300–400 °C and pressures of 40–50 bars. However, this process is not suited to produce ultra-low sulfur fuels that are necessary for the continuous operation of fuel cell applications.

Since most fuel processors and various fuel cell types are based on materials containing precious metal, for example, rhodium and platinum, sulfur content in the feed stock leads to rapid deactivation of the heterogeneous catalyst and to the loss of conversion efficiency. Even the normal odorous sulfur level in natural gas (4–6 ppmv; Knight and Verma, 1976) leads to a rapid deactivation of the reformer catalyst. Most fuel cell applications require sulfur contents below 0.1 ppmv (Chunshan, 2003; Hernandeza

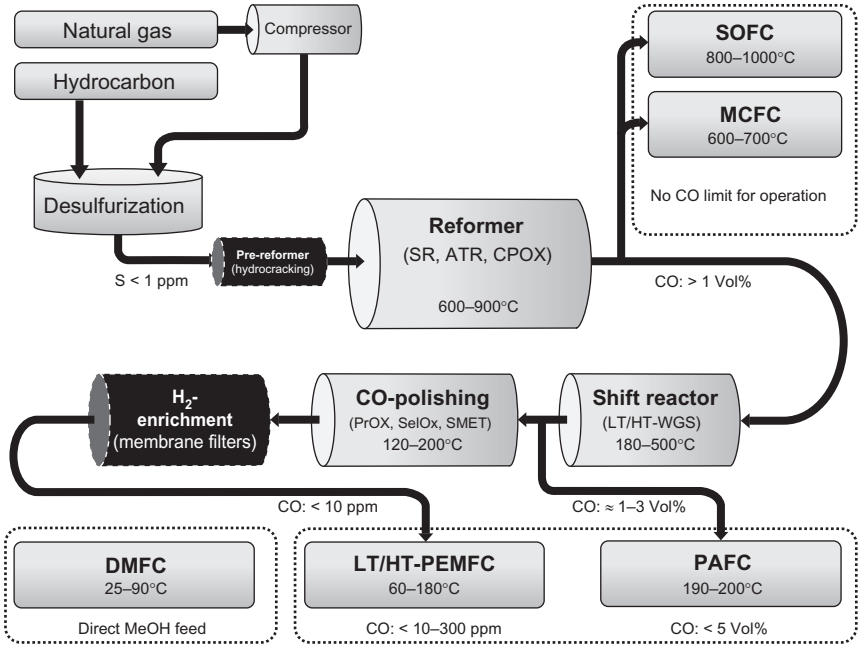

Figure 3 Scheme of the requirements of the fuel processing in order to meet the specific requirements of various fuel cells; adapted from Duisberg *et al.* (2008). Blackened parts are not necessary in general; their usage depends on the process demands due to fuel source and hydrogen quality.

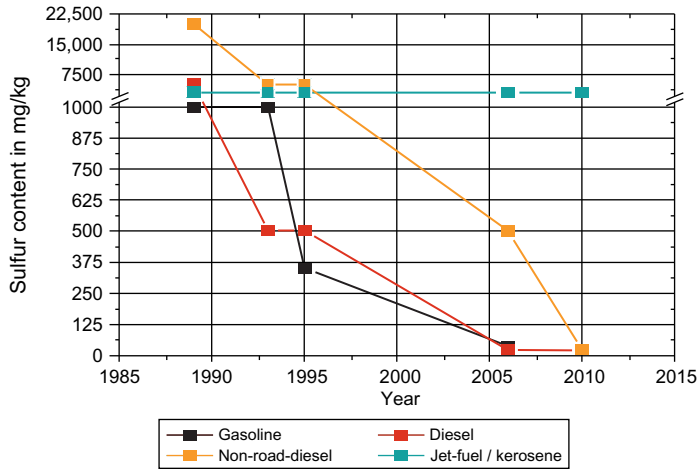

Figure 4 Sulfur levels in liquid fuels in relation to the directives of the EU and EPA, taken from van Rheinberg *et al.* (2011).

et al., 2008). Several technologies are available to provide ultra-clean hydrocarbon primary fuels, but it has become apparent that adsorptive desulfurization technologies are the best in terms of cost (van Rheinberg *et al.*, 2011). Adsorptive desulfurization is a widely used technology for the removal of sulfur from fuels to a level of ultra-clean quality. Simplicity and adaptability make this technology flexible and easy to integrate into the process due to the fuel processor and fuel cell type. A broad variety of sorbent materials are available on the market, ranging from zeolites and activated carbon over catalysts containing transition and precious metals to metal oxides, for example, ZnO. Actual research focuses on the development of more sulfur-tolerant catalyst systems for fuel processors and anode materials for fuel cells, requiring less precleaning of the fuel and thereby minimizing the balance of plant (BOP) and cost reduction.

Pre-reforming is performed to crack higher hydrocarbon species into hydrocarbons ranging from C_1 to C_6 as they have better reforming characteristics in ATR compared to long-chain and aromatic compounds (Borup *et al.*, 2005). Muradov *et al*. have reported about a novel combined pre-reforming–desulfurization process for the conversion of high-content sulfur diesel fuel to hydrogen-rich reformat suitable for fuel cells (Muradov *et al.*, 2010). The pre-reformer uses hydrogen recycled from the fuel processor/purification unit to convert sulfur-enriched diesel fuel (3180–5240 ppmw) into short-chain hydrocarbons, mainly propane, and H_2S. Muradov *et al*. assume that 13–16% of the hydrogen fraction needs to be used for recycling in their pre-reformer unit in order to convert diesel fuel to propane and butane. As pre-reforming catalyst, they use a mixture of zeolite and Ni-Mo/alumina catalyst at 400–500 °C with pressures around 14 bars. The desulfurization of the pre-reformer effluent gas was performed with adsorption technology using an aqueous ferric sulfate solution, which led to an overall desulfurization yield of 96–98%, with <5 ppmv H_2S content in the effluent gas. The process was operated for >100 h, and coke formation on the catalytic surface as well as deactivation of the pre-reformer was observed, depending on the process parameters. Since primary fuels are directly usable for reformer applications such as SR, ATR, or catalytic partial oxidation (CPOX), only desulfurization is necessary to protect the sulfur-sensitive active sites in most reforming catalyst. Pre-reforming appends another reactor unit to the complete fuel processor system and their application is doubtful due to coking/regeneration, volume, and weight increase in mobile applications.

4.2 Conversion of hydrocarbon fuels to hydrogen

The reactants in fuel processing, that is, the fuel $C_xH_yO_z$, steam, H_2O, and the oxidizer, O_2, contain carbon (C), hydrogen (H), and oxygen (O) atoms. From the point of thermodynamic equilibrium, a convenient way for

characterizing the feed composition is the specification of the molar ratios of the elements in the feed stream, which are usually expressed by the carbon-to-oxygen ratio (C/O),

$$\frac{\mathrm{C}}{\mathrm{O}} = \frac{x\dot{n}_{\mathrm{C}_x\mathrm{H}_y\mathrm{O}_z}}{2\dot{n}_{\mathrm{O}_2} + z\dot{n}_{\mathrm{C}_x\mathrm{H}_y\mathrm{O}_z}}, \tag{5}$$

and the steam-to-carbon ratio (S/C),

$$\frac{\mathrm{S}}{\mathrm{C}} = \frac{\dot{n}_{\mathrm{H}_2\mathrm{O}}}{x\dot{n}_{\mathrm{C}_x\mathrm{H}_y\mathrm{O}_z}}. \tag{6}$$

Sometimes, the oxygen content in the fuel is neglected in the computation of C/O.

The major global reactions occurring in fuel processing of hydrocarbon fuels $\mathrm{C}_x\mathrm{H}_y\mathrm{O}_z$ are:

SR:

$$\mathrm{C}_x\mathrm{H}_y\mathrm{O}_z + (x-z)\mathrm{H}_2\mathrm{O} \rightarrow x\mathrm{CO} + (x - z + y/2)\mathrm{H}_2, \quad \Delta H^0_{298} > 0 \tag{7}$$

POX:

$$\mathrm{C}_x\mathrm{H}_y + \frac{x}{2}\mathrm{O}_2 \rightarrow x\mathrm{CO} + \frac{y}{2}\mathrm{H}_2, \quad \Delta H^0_{298} < 0 \tag{8}$$

$$\mathrm{C}_x\mathrm{H}_y\mathrm{O}_z + \frac{(x-z)}{2}\mathrm{O}_2 \rightarrow x\mathrm{CO} + \frac{y}{2}\mathrm{H}_2, \quad \Delta H^0_{298} < 0 \tag{9}$$

total oxidation (combustion):

$$\mathrm{C}_x\mathrm{H}_y\mathrm{O}_z + \left(x - \frac{z}{2} + \frac{y}{2}\right)\mathrm{O}_2 \rightarrow x\mathrm{CO}_2 + \left(\frac{y}{2}\right)\mathrm{H}_2\mathrm{O}, \quad \Delta H^0_{298} \ll 0 \tag{10}$$

dry reforming (DR):

$$\mathrm{C}_x\mathrm{H}_y\mathrm{O}_z + (x-z)\mathrm{CO}_2 \rightarrow (2x-z)\mathrm{CO} + \frac{y}{2}\mathrm{H}_2, \quad \Delta H^0_{298} > 0 \tag{11}$$

WGS reaction:

$$\mathrm{CO} + \mathrm{H}_2\mathrm{O} \rightarrow \mathrm{CO}_2 + \mathrm{H}_2, \quad \Delta H^0_{298} = -41\,\mathrm{kJ\,mol^{-1}} \tag{12}$$

methanation

$$\mathrm{CO} + 3\mathrm{H}_2 \rightarrow \mathrm{CH}_4 + \mathrm{H}_2\mathrm{O}, \quad \Delta H^0_{298} = -206\,\mathrm{kJ\,mol^{-1}} \tag{13}$$

Boudouard reaction

$$2\mathrm{CO} \rightarrow \mathrm{C} + \mathrm{CO}_2, \quad \Delta H^0_{298} = -172\,\mathrm{kJ\,mol^{-1}}. \tag{14}$$

The combination of SR and POX is called ATR:

$$C_xH_yO_z + nO_2(x-z) + H_2O \rightarrow xCO_2 + \left(x - z + \frac{y}{2}\right)H_2, \quad \Delta H^0_{298} \sim 0. \qquad (15)$$

In reality, the reactions proceed via a complex network of elementary reactions and are often both in the gas phase and on the catalyst. Indeed, most of the fuel processing devices use heterogeneous catalysis, that is, the chemical conversion is carried out on the surface of a solid material, the catalyst. However, since most reforming processes are conducted at temperatures above 400 °C and sometimes even above 1000 °C (POX, ATR), homogeneous conversion in the gas phase can accompany the catalytic conversion. The potential products of gas-phase reactions may be quite different from the ones obtained over the catalyst. The formation of methane and light olefins are of particular interest. The latter ones may undergo molecular growth processes leading to polyaromatic hydrocarbons (PAHs) and finally to soot particles and coke layers on the catalysts and the solid walls of the apparatus and pipes (Kaltschmitt *et al.*, 2011).

SR is the highly endothermic conversion of any hydrocarbon species by steam into a mixture of carbon monoxide and hydrogen, the synthesis gas. The product stream usually also contains unconverted steam and some fuel and carbon dioxide, the latter due to consecutive WGS. Even though SR requires the supply of steam and heat, it has been the primary route for the production of hydrogen and synthesis gas. A major advantage of SR in comparison to POX and ATR is the fact that no oxygen is needed, and therefore nitrogen does not need to be pumped through the process in case oxygen is provided in form of air.

POX offers a possibility to run the fuel processor without additional devices for providing heat and steam; aside from the fuel, only oxygen (air) is needed. Using noble metal catalysts such as rhodium—this process is called CPOX—the fuel can be converted within milliseconds. By recycling the steam containing exhaust gas of the fuel cell stack, the CPOX reformer could be operated as an ATR reformer. For start-up, the C/O ratio may be decreased ($C/O < 0.5$) to use the highly exothermic combustion reactions to heat up the reformer to its operating temperature of $\sim$1000 °C and also to avoid and/or burn any undesired deposits.

ATR, both by gas phase and catalytic conversion, has gained attraction in the last decades because, in principle, no external heat is required.

4.2.1 Natural gas

SR of natural gas is the major route for the production of hydrogen and synthesis gas in chemical industry (Rostrup-Nielsen, 1984):

$$CH_4 + H_2O \rightarrow CO + 3H_2, \quad \Delta H^0_{298} = 207\,\mathrm{kJ\,mol^{-1}}. \qquad (16)$$

Even though higher pressures favor the reverse reactions, industrial steam reformers work with pressures above 20 bars due to requirements of downstream processes. Hydrogen as a separate component of synthesis gas is largely used in the manufacturing of ammonia and in a variety of petroleum hydrogenation processes. SR is a very efficient technology for the production of hydrogen and synthesis gas from fossil fuels in large-scale facilities, reaching yields close to the thermodynamic equilibrium (Rostrup-Nielsen, 1984). Conventional steam reformers deliver relatively high concentrations of hydrogen at high fuel conversion. The molar S/C ratio usually exceeds 2.5. The excess steam supports the completion of the reaction and inhibits coke formation, but additional heat must be added (Trimm, 1997). The products of the reaction are controlled mainly by thermodynamics, which favor the formation of methane at lower temperatures and of hydrogen at higher ones.

SR is usually carried out over Ni-based catalysts (Rostrup-Nielsen, 1984). The very expensive noble metal rhodium has also been shown to be a very efficient SR catalyst (Schadel *et al*., 2009) and is not as sensitive to coking as Ni. Recently, direct synthesis of Ni-based hydrotalcite was used to prepare small Ni nanocrystals which can efficiently be applied for sorption-enhanced steam methane reforming (Ochoa-Fernandez *et al*., 2005).

POX and autothermal oxidation: Due to the expected increase in the use of natural gas as a feedstock for chemical industry and as a primary fuel for fuel cell applications and due to the fact that the required external energy supply is disadvantageous in small-scale operation units, the interest in autothermally operated reformers for the conversion of natural gas into synthesis gas and hydrogen will grow further.

Due to the pioneering work of the Schmidt group (University of Minnesota), CPOX (Deutschmann and Schmidt, 1998; Dissanayake *et al*., 1993; Hannemann *et al*., 2007; Hickman and Schmidt, 1992, 1993a; Horn *et al*., 2006; Schwiedernoch *et al*., 2003) of natural gas, here expressed in terms of the major natural gas constituent, methane,

$$CH_4 + \frac{1}{2}O_2 \rightarrow CO + 2H_2, \quad \Delta H^0_{298} = -36\,\mathrm{kJ\,mol^{-1}}, \tag{17}$$

has attracted much interest because of its potential to conduct the reaction autothermally in compact devices and without an additional water tank, which can also reduce the cost of small-scale and remotely operated devices for synthesis gas and hydrogen production. At short contact times over noble metal catalysts, CPOX can basically be used for all hydrocarbon fuels. The addition of steam (ATR), for instance coming from the fuel cell exhaust, increases the hydrogen yield,

$$CH_4 + \frac{1}{2}O_2 + H_2O \rightarrow CO_2 + 3H_2, \quad \Delta H^0_{298} = -76\,\mathrm{kJ\,mol^{-1}}. \tag{18}$$

POX of methane over rhodium-coated monoliths is one of the most studied systems in fuel processing for the production of hydrogen. In Section 6, we therefore use this process as an example to illustrate the state of the art in modeling fuel processors.

DR, using CO_2, is especially discussed in the context of the useful processing of a greenhouse gas in the chemical industry. Since the reaction is slow, it currently does not play any role in fuel processing for fuel cell applications.

4.2.2 Methanol

Steam reforming: The thermodynamic equilibrium composition of methanol–steam mixtures exhibits a maximum yield of H_2 at S/C $\sim$1. Potentially harmful by-products are formic acid (HCOOH) and methyl formate (CH_3-OCHO) (Takahashi *et al.*, 1985).

$$CH_3OH + H_2O \rightarrow CO_2 + 3H_2, \quad \Delta H^0_{298} = 50\,\mathrm{kJ\,mol^{-1}} \tag{19}$$

4.2.3 Ethanol

Due to the increasing use of biomass in the energy sector, conversion of ethanol to hydrogen has recently been extensively investigated by using SR (Birot *et al.*, 2008; Cavallaro, 2000; Cavallaro *et al.*, 2003a; Laosiripojana and Assabumrungrat, 2006; Liguras *et al.*, 2003; Liu *et al.*, 2008; Roh *et al.*, 2008; Wanat *et al.*, 2004), POX (Costa *et al.*, 2008; Salge *et al.*, 2005; Silva *et al.*, 2008a,b; Wanat *et al.*, 2005), and ATR (Akdim *et al.*, 2008; Cavallaro *et al.*, 2003b; Deluga *et al.*, 2004; Fierro *et al.*, 2003, 2005, 2002; Vesselli *et al.*, 2005).

SR of ethanol,

$$C_2H_5OH + H_2O \rightarrow 2CO + 4H_2, \quad \Delta H^0_{298} = +256\,\mathrm{kJ\,mol^{-1}}, \tag{20}$$

requires higher temperatures than methanol SR, which may also lead to ethanol decomposition (Fishtik *et al.*, 2000),

$$C_2H_5OH \rightarrow CH_4 + CO + H_2, \quad \Delta H^0_{298} = +49\,\mathrm{kJ\,mol^{-1}}, \tag{21}$$

and to the formation of numerous by-products, such as ethylene,

$$C_2H_5OH \rightarrow C_2H_4 + H_2O, \quad \Delta H^0_{298} = +45\,\mathrm{kJ\,mol^{-1}}, \tag{22}$$

and acetaldehyde,

$$C_2H_5OH \rightarrow CH_3CHO + H_2, \quad \Delta H^0_{298} = +69\,\mathrm{kJ\,mol^{-1}}. \tag{23}$$

POX,

$$C_2H_5OH + \frac{1}{2}O_2 \rightarrow 2CO + 3H_2, \quad \Delta H^0_{298} = +14\,\mathrm{kJ\,mol^{-1}}, \tag{24}$$

presents an alternate route for hydrogen production from ethanol, in particular with rhodium catalysts. POX of ethanol is slightly endothermic, a notable difference to POX of aliphatic hydrocarbons such as methane (natural gas), *iso*-octane (gasoline), and hexadecane (diesel). For C/O < 0.8, the selectivity to hydrogen is almost as high as in the thermodynamic equilibrium without by-product formation (Hebben *et al.*, 2010). At C/O > 0.8, the conversion of ethanol decreases while the oxygen conversion is complete. Significant amounts of methane, ethylene, acetaldehyde, and diethyl ether have been detected in CPOX of ethanol at C/O > 1.2 (Figure 5), which can be related to the accumulation of carbonaceous overlayers with time on stream (Hebben *et al.*, 2010).

4.2.4 Gasoline

SR of higher hydrocarbons, here given for *iso*-octane as a gasoline surrogate,

$$i\text{–}C_8H_{18} + 8H_2O \rightarrow 8CO + 17H_2, \quad \Delta H^0_{298} = +1274\,\mathrm{kJ\,mol^{-1}}, \tag{25}$$

requires high temperatures and is usually operated at S/C well above the stoichiometric ratio of S/C = 2 to avoid the formation of coke precursors, which reduces the overall efficiency of the process.

POX,

$$i\text{–}C_8H_{18} + 4O_2 \rightarrow 8CO + 9H_2, \quad \Delta H^0_{298} = -660\,\mathrm{kJ\,mol^{-1}}, \tag{26}$$

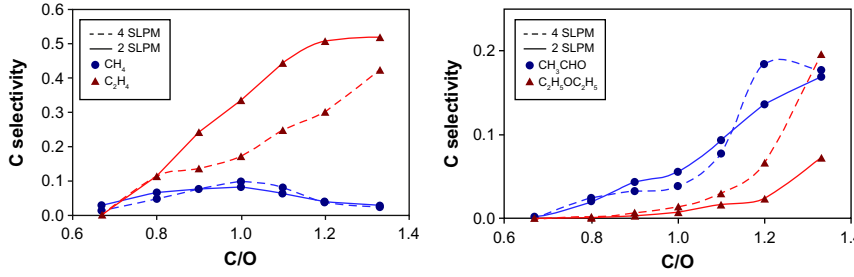

Figure 5 Experimentally measured selectivity of by-products as a function of C/O for the CPOX of ethanol on alumina-supported Rh-coated honeycomb catalysts for two different flow rates; taken from Hebben *et al.* (2010).

on the other hand, is a useful alternate route that has been the subject of several recent studies with the focus on auxiliary power unit (APU) on-board of vehicles.

However, the varying composition of logistic fuels such as gasoline, kerosene, and diesel challenges any model predictions of the performance of catalytic gasoline reformers. The composition does not only influence the overall hydrogen yield but also the propensity of the coke formation. A systematic study on the reforming of gasoline components over Rh/Al_2O_3-coated monoliths for a wide range of C/O ratios was recently conducted by Hartmann *et al.* (2009a). The impact of the chemical structure and chain length of hydrocarbons in CPOX over Rh-based catalysts has been studied, using benzene, cyclohexane, 1-hexene, and *i*-hexane (3-methylpentane) for the representation of archetypical constituents of logistic fuels (Hartmann *et al.*, 2009a). Since these species have the same number of carbon atoms, their performance can easily be compared on the basis of their molar C/O ratios. The influence of the fuel components is studied by comparison of a series of linear alkanes ranging from *n*-hexane to *n*-dodecane and thereby representing the wide range of boiling points of the individual fuel components. Furthermore, the effect of side chains of cyclic hydrocarbons has been studied by using species with methyl substitution of benzene and cyclohexane. This study revealed the dominant role of the structure of the hydrocarbon fuel (*n*-alkanes, *i*-alkanes, cycloalkanes, olefins, or aromatics) in the production of synthesis gas (Figure 6) and undesired by-products. Especially the presence of double bonds or an aromatic ring shifts the yield to total oxidation products.

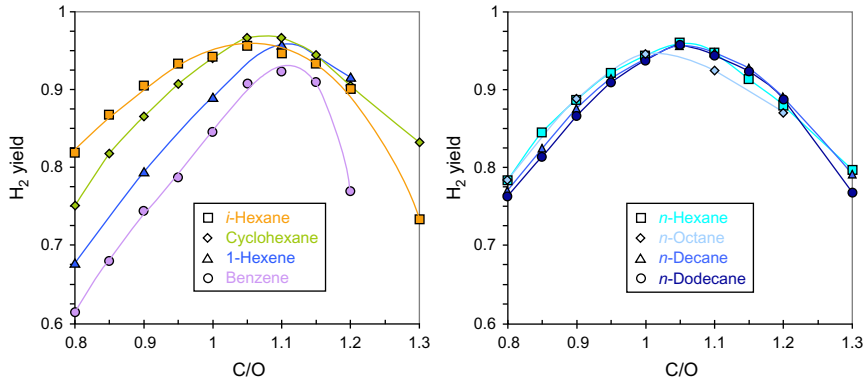

Figure 6 H_2 yields in CPOX of characteristic components of logistic transportation fuels over Rh/alumina-coated honeycomb catalysts as a function of C/O ratio; taken from Hartmann *et al.* (2009a).

On the other side, equivalent performance is observed for varying chain lengths of the hydrocarbon backbone or the appearance of side chains. Ethylene, propylene, and acetylene are precursors for coke formation in reforming processes (Kang *et al.*, 2010, 2011; Villano *et al.*, 2010). The propensity of the formation of these coke precursors is also dominated by the structure of the hydrocarbon fuel (Hartmann *et al.*, 2009a). Acetylene is exclusively found in conversion of aromatic hydrocarbons. Furthermore, acetylene is the only hydrocarbon cracking product formed under fuel lean conditions, which can be attributed to the high reaction temperatures reached in conversion of aromatic hydrocarbon fuels and by an excess of oxygen. The strong increase in formation of α-olefins with increasing C/O in CPOX of hydrocarbons can also be employed for application in chemical industry (Krummenacher and Schmidt, 2004).

Based upon the knowledge of the reaction of characteristic fuel constituents, surrogates of logistic fuels can be obtained. Besides the reduction of the high complexity of commercial fuels in model fuels, the use of surrogates allows a reliable standardization and reproduction of CPOX experiments. Moreover, the influence and interaction of dominant constituents can be explored, allowing the development of detailed models for CPOX of logistic fuels.

Gasoline/ethanol mixtures: The characteristic features of ethanol reforming lead to the question of their impact on the reforming of gasoline that is blended with ethanol. The increasing use of renewable fuels, for example, ethanol, and fossil fuels blended with renewable fuels, for example, E10, in vehicles also intensifies the research activities for these fuels in the field of on-board hydrogen supply (Cavallaro *et al.*, 2003a; de Lima *et al.*, 2009; Deluga *et al.*, 2004; Fatsikostas *et al.*, 2002; Hebben *et al.*, 2010; Hohn and Lin, 2009; Kirillov *et al.*, 2008; Liguras *et al.*, 2004; Ni *et al.*, 2007; Nilsson *et al.*, 2008; Sato *et al.*, 2010). In a recent study, Diehm (2010) systematically studied the impact of ethanol content in gasoline on CPOX of gasoline over a Rh/alumina-coated monolith. Using ethanol/*i*-octane as surrogate, it was observed that the conversion of ethanol is faster than that of *iso*-octane (Figure 7). In particular, the conversion of *iso*-octane already drops at relatively low C/O ratios, and increasing ethanol content intensifies this effect. The hydrogen selectivity generally decreases with increasing ethanol content; however, this trend is not linear. In fact, the highest hydrogen yield is achieved at 5% ethanol and not at pure *iso*-octane (Figure 7). The formation of by-products is also promoted by ethanol, and rather high ethylene concentrations are found even at low C/O ratios. All these findings were also observed using ethanol blended with commercial gasoline (E5, E10, E85) (Diehm, 2010), which implies that ethanol-blended *iso*-octane can serve as a surrogate for ethanol-blended gasoline.

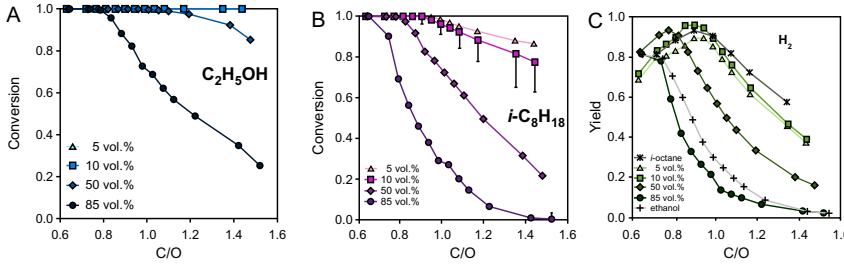

Figure 7 C-based conversion of ethanol (A) and *iso*-octane (B), and hydrogen yield (C) as a function of the C/O ratio for CPOX of ethanol/*iso*-octane blends over a Rh/Al_2O_3-coated honeycomb monolith. Vol.% nomenclature denotes the molar percentage of ethanol in the blend. Taken from Diehm (2010).

4.2.5 Diesel

In comparison to natural gas and gasoline, diesel fuel has the higher hydrogen energy density. However, diesel is the more difficult fuel to reform because diesel fuel is a mixture of a wide variety of paraffins, naphthenes, and aromatics, each of which reacts differently in a CPOX reaction, as discussed above and elsewhere (Hartmann *et al.*, 2009a; Shekhawat *et al.*, 2009; Subramanian *et al.*, 2004). The usual occurrence of organosulfur compounds will complicate the reforming even more, in particular concerning catalyst deactivation.

Rhodium-based catalysts were chosen for many studies of catalytic reforming of diesel and its major components, not only because it was successfully applied for reforming, in particular CPOX, of lighter hydrocarbons but also because it revealed low propensity for carbon formation (Krummenacher and Schmidt, 2004; Krummenacher *et al.*, 2003; O'Connor *et al.*, 2000; Shekhawat *et al.*, 2006; Subramanian *et al.*, 2004; Thormann *et al.*, 2009, 2008b). The study of Krummenacher *et al.* (2003) on CPOX of diesel over Rh/Al_2O_3-coated foam catalysts revealed that the highest hydrogen yields can be achieved when the reactor is operated at low C/O ratios, which are actually close to the flammability of the mixture shown in Figure 8. Furthermore, the operation of diesel fuel at such low C/O ratios presents a challenge for the mixing and feeding of the reactants, and in particular, a much higher tendency to precombustion of the fuel upstream the catalytic section is observed. This transient behavior is less drastic when the single fuel components or their binary mixtures are used. The hydrogen yields show a maximum at C/O ratios closer to 1.0, and the reactor can be operated more safely (Hartmann *et al.*, 2009a; Krummenacher and Schmidt, 2004; Krummenacher *et al.*, 2003).

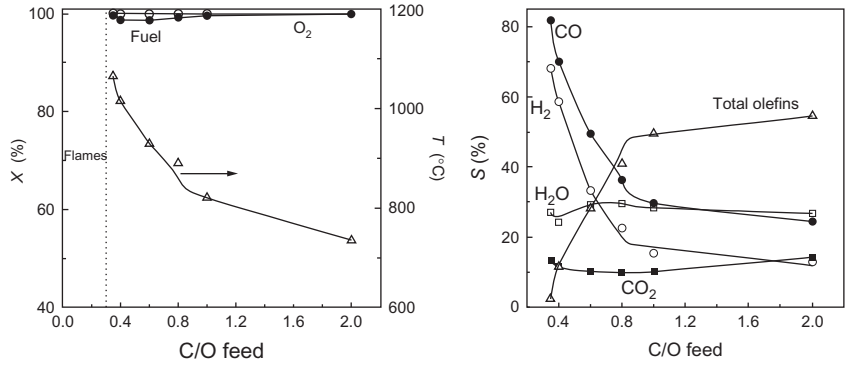

Figure 8 Effect of the C/O ratio on the partial oxidation of diesel fuel over a Rh/alumina-coated foam catalyst; conversion of fuel and oxygen, and catalyst exit temperature measured (left) and product selectivity (right); taken from Krummenacher *et al*. (2003).

CPOX of diesel is also more affected by the formation of carbonaceous overlayers and coking of the reactor lines downstream of the catalyst. Indeed, incomplete conversion of the fuel in the catalytic section will eventually lead to coke formation, unless secondary measures are applied. Since oxygen consumption is usually complete, the C/O ratio moves to infinity along the reactor. The pyrolytic conditions will eventually lead to the production of the coke precursors: ethylene and propylene. Even when the production of the olefins is on a ppm level, the accumulative effect may lead to coking problems after a certain time of operation of a technical system.

Aside from pure CPOX operation, the addition of steam and/or exhaust of, for instance, a downstream-operated fuel cell stack may be beneficial not only to efficiency due to improved heat balances but also to prevention of coking. However, it has to be taken into account that the oxygen in H_2O and CO_2 may reveal a different reactivity than the oxygen of molecular O_2 (Kaltschmitt *et al*., 2012).

ATR, and SR even more, moves the operation away from the coking region, which was also observed by Thormann *et al*. (2009, 2008a,b) for SR of diesel and hexadecane over Rh/CeO_2 catalysts in a microreactor.

4.3 Product clean-up and optimization—Shift catalysts and CO polishing

Syngas produced from a hydrocarbon fuel source contains hydrogen, carbon monoxide, water, and carbon dioxide as major components, depending on the fuel-to-oxygen (C/O) ratio at which the fuel processor is operated.

Using such kind of syngas for fuel cell application, further final conditioning of the syngas is required for maximum fuel cell power output.

High-temperature fuel cells such as solid oxide fuel cell (SOFC) and molten carbonate fuel cell (MCFC) are insensitive to CO and can convert both H_2 and CO to electrical power. The removal of CO in the syngas is vital for polymer electrolyte fuel cells, because blockage of the active sites in the anode material (often platinum) occurs due to the low operation temperature. Typically, CO conditioning down to <10 ppm levels has to be realized when providing a hydrogen-rich syngas derived from a primary fuel. Technologies for CO removal from the syngas fuel stream are the WGS reaction, preferential oxidation (PrOX), selective methanation of CO (SMET), and membrane filters.

The WGS reaction is a well-known process technology used in industrial and refinery scale. Conventional WGS can be processed in two stages: a high-temperature stage (HTS), using Fe–Cr-based catalysts, and a low-temperature stage (LTS), using Cu–Zn–Al_2O_3-based catalysts. Combining both stages can reduce the CO content in the gas stream down to approximately 1 vol.% at a relevant temperature of about 200 °C. The WGS reaction is an equilibrium-controlled, mildly exothermic reaction. Therefore, the H_2 content in the syngas, S/C ratio, and temperature have significant influence on the equilibrium. A critical review on WGS catalysis is provided by Ratnasamy and Wagner (2009). In terms of fuel cell application, precious metal catalysts are of great interest due to their much higher activity compared to the conventional catalyst systems. Therefore, they reduce catalyst bed volume and weight, and make the overall process more economical. Ceria- and titanium-supported platinum catalysts have been studied extensively (Ghenciu, 2002; Ratnasamy and Wagner, 2009; Ruettinger *et al.*, 2006), operating in a temperature regime of about 250–400 °C. Pd–Zn-based (250–300 °C) (Dagle *et al.*, 2008) and Au-based catalysts (150–250 °C) (Ratnasamy and Wagner, 2009; Senanayake *et al.*, 2009; Zane *et al.*, 2009) are promising catalyst systems on WGS reaction but industrial stage has not yet been reached.

High-temperature WGS is usually operated in a temperature range of about 320–450 °C and removes CO down to a level of 3–4 vol.% (dry basis) in the effluent. The temperature should not exceed 500 °C to avoid catalyst sintering. Small amounts of sulfur contained in the feed stream of <100 ppm are tolerated by conventional Fe-based catalyst systems.

Low-temperature WGS is operated in a temperature range of about 180–240 °C due to sintering of the Cu sites and lowering Cu dispersion. LTS typically reduces the CO content in the effluent of a HTS down to 0.3–1 vol.% due to the temperature limitations of commercial available Cu–Zn catalysts. For PEMFC usage, this content is still too high and further CO removal has to be carried out.

Preferential oxidation of carbon monoxide (PrOX) has been considered a promising technology for CO removal to reach CO concentrations below 10 ppm in order to meet requirements for PEMFC operation in nonstationary applications (Bion *et al.*, 2008). Originally, Pt-based catalysts were used for selective oxidation of CO in the presence of hydrogen (Park *et al.*, 2009). Later on, Oh and Sinkevitch reported that Ru/Al_2O_3 and Rh/Al_2O_3 were more selective catalyst systems compared to Pt/Al_2O_3 (Oh and Sinkevitch, 1993). Today, several metal oxide catalyst systems are under investigation, which are more active for the oxidation of CO than H_2. $CuO–CeO_2$ has been reported to be quite active for PrOX, with high CO conversion up to 99%. Accurate preparation methods and preconditioning parameters have to be followed since the reduction/oxidation processes on both cupper and ceria are responsible for the high activity of these catalysts (Avgouropoulos and Ioannides, 2006). Au-based catalysts show high conversion in PrOX at low temperatures, but no catalyst has been reported to show activity stable enough to meet acceptable CO conversion over a longer period of time under realistic reaction conditions (Bion *et al.*, 2008). Monometallic platinum catalysts show noticeable activity in PrOX at temperatures above 150 °C. Nevertheless, complete removal of CO cannot be accomplished due to the platinum activity in reverse WGS chemistry at temperatures above 150 °C (Bion *et al.*, 2008). Several types of platinum and other noble metal-based (Rh, Ru, and Pd) catalysts on different supports (alumina, silica, and zeolites) have been reported, but only a few have been identified to reach acceptable CO conversion with a wide temperature window under realistic reaction conditions. A review on recent catalyst systems was given by Park *et al.* (2009) and Bion *et al.* (2008).

Selective methanation of CO and H_2 selective membranes are another possibility to remove CO from the reformer effluent gas (Park *et al.*, 2009). Selective methanation can be carried out over various hydrogenation catalysts in the presence of CO, CO_2, and H_2. Since the methanation reaction is highly exothermic, precise temperature control of the process is crucial, otherwise reverse WGS can occur at high resident times. Ru and Rh supported on alumina are reported to be good catalysts for selective methanation even in the presence of CO_2. Furthermore, Ni-based catalysts have been tested with high activities. Takenaka *et al.* showed that a reduction of 0.5 vol.% down to 20 ppm CO is possible (Takenaka *et al.*, 2004). Nevertheless, CO concentrations below 10 ppm were not reachable with selective methanation.

Pressure swing adsorption for gas purification is often performed in large-scale stationary plant processing. Since this is no technology for small-scale fuel cell applications, no more attention is paid to this.

5. CURRENT TECHNOLOGIES

In this subsection, we describe a few recent developments in the field of complete fuel processor—fuel cell—power unit as well as already commercialized systems; this is not, by any means, a complete overview. Independent of a special reformer unit, some requirements have to be met. In aviation, applications reliability and efficiency are the major requirements in connection with a reformer unit, whereas in automotive applications, a compact size and weight reduction are important. Applications for undersea and/or aerial vehicles have to meet all four requirements. Since there is no commercialized product on the market, which meets all mentioned points, further R&D is needed both on catalyst improvements and reaction engineering, supported by mathematical modeling.

5.1 Field of application

Depending on the power size of the fuel cell stack, different fields of application can be identified. They can be roughly divided into five different applications on the basis of their electrical power demand.

The most common usage of a fuel processor/fuel cell unit is in large-scale power plants, where they are operated in the MW range for on-site power and grid support. The plant consists of a complete fuel processing system, including fuel storage, fuel reformer, gas clean-up, fuel cell assembly, and DC/AC converter unit. Commercial fuel cell stacks integrated in such plants are already commercially available and generate about 181 MW overall electrical power in the USA. Commercialized products currently available on the market in size of power plant classification are, for instance, DirectFuelCell® and PureCell®. Both technologies operate with SOFC or MCFC units for electricity production, combined with either a natural gas or a liquefied natural gas steam reformer.

A second prevalent field of application is the usage in back-up systems. The fuel cell unit is coupled in parallel to the existing power supply, charging batteries or supplying electrical power in case of power outage. Typical power supply is several kW, produced mainly from compressed hydrogen with PEMFC.

Combined heat and power systems are designed for residential usage in houses and buildings. Waste heat of the SOFC unit is used for water boiling, coming up with an thermal efficiency of 90% (Kleiber-Viglione, 2011) compared to about 30–40% electrical efficiency of the fuel cell stack itself (Wendt, 2005). For residential application, natural gas or LPG is the preferential primary fuel, combined with an ATR.

Ceramic Fuel Cells Limited's BlueGen® technology is a commercialized product in this field of application, which is sold in the European and US market (Rowe and Karl, 2011).

In the field of mobile applications, APUs are under rapid development by industry and research science. Their electrical power ranges from 1 to 5 kW, in special cases even up to 500 kW. APUs consist of an on-board reformer coupled to a fuel cell and are operated with liquid hydrocarbons, mainly diesel fuel, carried on-board of the vehicle. Currently, inefficient electricity generation is applied by idling of the internal combustion engine, by which one billion gallons of diesel fuel (Mintz *et al.*, 2000) are consumed annually in the USA. The main problems preventing commercialization still are the coking behavior of such systems fuelled with liquid hydrocarbons, thermal management including the long start-up period, and the sulfur content in the fuel. New developments are under construction and were successfully tested in different mobile applications, for instance Delphi Corp. US and AVL List GmbH got their APU systems to field test status (Hennessy, 2011; Rechberger, 2011). With, for example, SchIBZ (e4ships 2009) and MC-WAP (CETENA S.p.A. 2004), two international projects are dealing with the development of diesel-powered 500 kW APU systems for maritime application using SOFC and MCFC fuel cells.

The last identified field of application deals with the replacement of conventional batteries with portable electronics, and with, for example, lift trucks in the section for material handling equipment. Power packs for consumers based on DMFCs, ranging from mW to a scale of several Watt, can be used for mobile computing and cell phone charging but are only available on research level so far. Micro fuel cell technology is used to reduce reformer/fuel cell volume and weight. For PEMFCs, Ballard FCGen® and FCvelocity™ fuel cell stacks (Plug and Power GenDrive™) are widely used in the USA for lift trucks, combined with a compressed hydrogen tank (Simon, 2011). Apart from the PEMFC stack itself, research is performed on the water handling issues for these fuel cell types. Typical problems include flooding of the fuel cell exhaust with produced water.

Air-independent power and energy solutions are developed for strategic autonomous undersea vehicles. Due to their small size, low weight, and reliability, PEMFC and DMFC are under development. Fast and simple start-up is achieved by providing H_2 from liquid metal hydride solutions, for example, $NaBH_4$, $LiAlH_4$, and O_2 from liquid oxygen (Fontaine, 2011).

5.2 Fields of application for fuel cell types

For each application, specified boundary conditions have to be taken into account when choosing the type of fuel cell. SOFC and MCFC have high working temperatures above 600 °C and need thermal management and

an efficient BOP. Therefore, these types of fuel cells are normally used with fuel processors, generating waste heat and a hot reformat gas which is used to supply the fuel cell stack with heat. Due to the high temperature, these types of fuel cells are insensitive to carbon monoxide in the reformate and handle most syngas reformates produced typically for SR, ATR, and CPOX fuel processors without further CO clean-up/polishing. Nevertheless, desulfurization has to be carried out to protect the reforming catalysts from poisoning.

PEMFCs are usually used in the power range of a few watts to several kW, depending on the application. In most available systems, compressed hydrogen is used as feed fuel, stored in a tank next to the fuel cell stack. No further gas purification is needed since no primary fuel source is used. Otherwise, desulfurization and CO clean-up have to be taken into account when using PEMFC stacks. PEMFCs are normally operated in the temperature range of 60–120 °C. High-temperature PEMFCs can be used up to 180 °C, depending on the electrolyte used in the cell. PEMFCs have a stringent demand on CO removal down to 10 ppm or less for stable operation. High-temperature PEMFCs can handle up to 100 ppm CO content in the feed gas.

For a smaller power demand, DMFCs are mainly used in the power range of 1 mW to about 20 W for portable electronics power packs. Using microreactor technology, a compact design and low weight can be achieved with operational temperatures from room temperature up to 90 °C. Methanol has to be contained in the fuel cell system.

5.3 Balance of plant

For a fully operational fuel processor system, not only the reformer and the fuel cell stack are relevant; instead, multiple components are needed around the reformer/fuel cell assembly such as sensors, electronic controls, pumps, start-up power sources, burners, heat exchangers, steam generators, sulfur removal units, water recovery unit, thermal insulation, and filters. Since this section gives a short overview, technical specifications of each component are not mentioned. Nevertheless, as fuel processing is sensitive to the maintaining of constant flow rates and ratios of fuel/air/steam for high efficiency, high demands are made on each component. Especially at high temperatures, accurate flow control is essential to avoid temperature drift or peaks in order to observe material limits and safety issues.

The BOP can roughly be divided into three sections: upstream and downstream of the reformer/stack unit, and the control system. The fuel feed management consists of fuel pumping, atomization, evaporation, air control, and homogeneous mixing of the reactants to provide accurate

pulse-free feed flows. In case of gaseous fuels, flow control is quite easy to handle, whereas atomization, evaporation, and mixing of liquid fuels in air are more challenging. Fuel breakthrough and precombustion of the fuel have to be avoided when it is mixed with air, otherwise coking of the reformer system and of the downstream fuel cell stack is unavoidable, which will lead to system failure in the end. Depending on the fuel cell stack, the reformat temperature has to be controlled for downstream shift, PrOX reactors, or fuel cells with lower operation temperature. Several heat exchanges can be implemented in a fuel processor system, recycling energy by preheating inlet flows from the hot anode exhaust gas stream or condensing steam for water recycling. In high-temperature fuel cells, even the cathode air stream has to be preheated to avoid thermal shock of the stack, but energy still has to be taken out of the stack to prevent overheating. Especially in high-temperature fuel cells, high demands are made on insulation materials since most pumps, blowers, and end electronic components are not suitable for higher temperature environments. Ceramic materials such as zirconia, alumina, and silica are often used as insulation materials due to their low thermal conductivity and weight. For a successful commercial implementation of fuel processor systems, a sophisticated BOP of the various components is necessary.

6. APPROACHES FOR MODELING FUEL PROCESSING

This section focuses on the modeling and simulation approaches for analyzing heterogeneously catalyzed gas-phase reactions and their interaction with the surrounding flow field, as occurring in fuel reformers for the production of hydrogen and hydrogen-rich synthesis gases. Understanding and optimization of these heterogeneous reactive systems require the knowledge of the physical and chemical processes taking place on a molecular level. In particular at short contact times and high temperatures, reactions occur on the catalyst and in the gas phase. Consequently, the interactions of mass and heat transport with heterogeneous and homogeneous chemistries become even more important.

Monolithic reactors are frequently used for SR, POX, and ATR of hydrocarbon fuels and can therefore serve as an example. Figure 9 illustrates the physical and chemical processes in a high-temperature catalytic monolith that glows at a temperature of around 1000 °C due to the exothermic oxidation reactions. In each channel of the monolith, the transport of momentum, energy, and chemical species occurs not only in flow (axial) direction, but also in radial direction. The reactants diffuse to the inner channel wall, which is coated with the catalytic material, where the gaseous species adsorb and react on the surface. The products

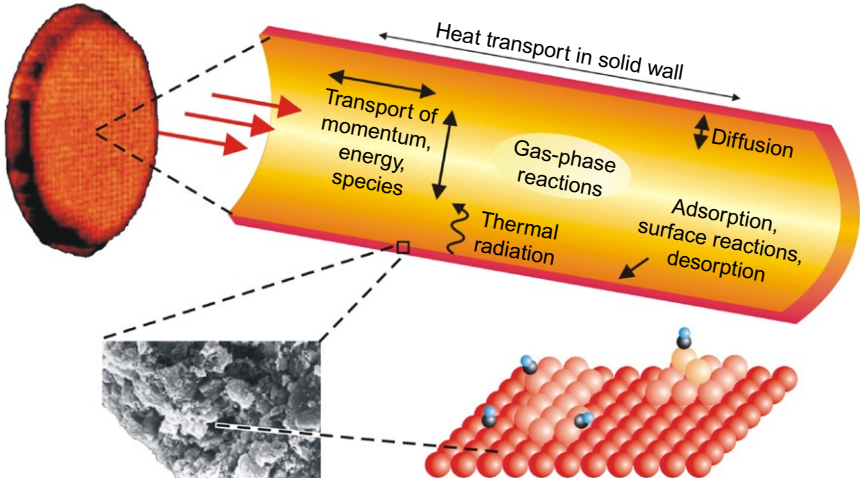

Figure 9 Sketch of the physical and chemical processes occurring in a catalyst-coated honeycomb monolith. Many length and time scales have to be considered simultaneously reaching from a scale of nanometer and picosecond (e.g., surface reactions), to one of micro/millimeter and micro/millisecond (e.g., internal/external diffusion), and to one of centimeter and second (e.g., heat transport in solid structures); taken from Janardhanan and Deutschman (2011).

and intermediates desorb and diffuse back into the bulk flow. Due to the high temperatures, the chemical species may also react homogeneously in the gas phase. In catalytic reactors, the catalyst material is often dispersed in porous structures such as washcoats or pellets. Mass transport in the fluid phase and chemical reactions are then superimposed by diffusion of the species to the active catalytic centers in the pores. The temperature distribution depends on the interaction between heat convection and conduction in the fluid, heat generation/consumption due to chemical reactions, heat transport in the solid material, and thermal radiation. Both variation of the feed conditions in time and space and heat transfer between the reactor and the ambience result in a nonuniform temperature distribution over the entire monolith, which means that the behavior will differ from channel to channel (Windmann *et al.*, 2003).

The challenge in catalytic fuel processing is not only the development of new catalysts to obtain the desired product, but also the understanding of the interaction of the catalyst with the surrounding reactive flow field. Sometimes, the use of these interactions alone can lead to the desired product selectivity and yield. For detailed introductions into transport phenomena and their coupling with heterogeneous reactions, readers are

referred to references (Bird *et al.*, 2001; Hayes and Kolaczkowski, 1997; Kee *et al.*, 2003; Patankar, 1980; Warnatz *et al.*, 1996) and (Deutschmann, 2008, 2011; Kee *et al.*, 2003), respectively.

In the remainder of this section, the individual physical and chemical processes and their coupling will be discussed, beginning with the reactions on the solid catalyst.

6.1 Modeling the rate of heterogeneous catalytic reactions

The understanding of the catalytic cycle in fuel reformers is a crucial step in reformer design and optimization. The development of a reliable surface reaction mechanism is a complex process, which is today increasingly based on the elucidation of the molecular steps. A survey on state-of-the-art modeling of heterogeneously catalyzed gas-phase reactions can be found in Deutschmann (2011).

The catalytic reaction cycle can be expressed by a heterogeneous reaction mechanism, which consists of a set of K_s chemical reactions among N_g gas-phase species, N_s species adsorbed on the top catalyst layer, and N_b bulk species absorbed by the catalyst particle; species name is denoted by A_i:

$$\sum_{i=1}^{N_g+N_s+N_b} \nu'_{ik} A_i \rightarrow \sum_{i=1}^{N_g+N_s+N_b} \nu''_{ik} A_i, \tag{27}$$

with ν'_{ik}, ν''_{ik} being the stoichiometric coefficients. In technical systems, the mean-field (MF) approximation is the most frequently applied approach for calculating the chemical reaction rates of the individual reactions in the mechanism (Deutschmann, 2008). In this concept, the local reaction rate is related to the size of the computational grid in the flow field simulation, assuming that the local state of the active surface can be represented by mean values for the cells of the computational grid. Hence, this model does not resolve any spatial inhomogeneity in this cell on the catalytic surface as Monte-Carlo simulation would do. In the MF approximation, the state of the catalytic surface is described by the temperature T and a set of surface coverages θ_i, which is the fraction of the surface covered with surface species i. The surface temperature and the coverage depend on time and the macroscopic position in the reactor, but are averaged over microscopic local fluctuations. The local chemical source term, R_i^{het}, is derived from the molar net production rate, $\dot{s}_i$, by

$$R_i^{\text{het}} = \eta F_{\text{cat/geo}} \dot{s}_i M_i = \eta F_{\text{cat/geo}} M_i \sum_{k=1}^{K_s} \nu_{ik} k_{f_k} \prod_{j=1}^{N_g+N_s+N_b} c_j^{\nu'_{jk}}. \tag{28}$$

Here, K_s is the number of surface reactions, c_i are the species concentrations, which are given, for example, in mol m^{-2} for the N_s adsorbed species and in mol m^{-3} for the N_g and N_b gaseous and bulk species.

The molar net production rate of gas-phase species i, $\dot{s}_i$, given in mol m^{-2} s^{-1}, refers to the actual catalytically active surface area, that is, the (crystal) surface of the catalyst particle, which usually has the size of 1–10^3 nm. These catalyst particles are usually dispersed in a certain structure, for instance, they may occur as dispersed particles on a flat or in a porous substrate or pellet. The simplest way to account for this structure and the total active catalytic surface area in a reactor simulation is the scaling of the intrinsic reaction rate at the fluid–solid interphase by two parameters. The first parameter, $F_{cat/geo}$, represents the amount of the total active catalytic surface area in relation to the geometric surface area of the fluid–solid interphase. Recently, it has been shown that this ratio ($F_{cat/geo}$) can also serve as a parameter to describe the dependence of the overall reaction rate on catalyst loadings and on effects of hydrothermal aging for structure-insensitive catalysts (Boll *et al.*, 2010). An alternate representation of the total catalytic surface area is the volume-specific catalyst surface area, which is related to the reactor or porous media volume.

The simplest model to include the effect of internal mass transfer resistance for catalysts dispersed in a porous media is the effectiveness factor, η_i, based on the Thiele modulus (Hayes and Kolaczkowski, 1997; Papadias *et al.*, 2000). In case of infinite fast diffusion of reactants and products in the porous structure, the effectiveness factor becomes unity.

According to Equation (28) and the relation $\Theta_i = c_i \sigma_i \Gamma^{-1}$, the variations of surface coverage follow

$$\frac{\partial \Theta_i}{\partial t} = \frac{\dot{s}_i \sigma_i}{\Gamma}. \tag{29}$$

Here, the coordination number σ_i gives the number of surface sites which are covered by the adsorbed species. Since the binding states of adsorption of all species vary with the surface coverage, the expression for the rate coefficient, k_{f_k}, is commonly extended by coverage-dependent parameters $\mu_{i_k}$and ε_{i_k} (Coltrin *et al.*, 1991; Kee *et al.*, 2003):

$$k_{f_k} = A_k T^{\beta_k} \exp\left[\frac{-E_{a_k}}{RT}\right] \prod_{i=1}^{N_s} \Theta_i^{\mu_{i_k}} \exp\left[\frac{\varepsilon_{i_k} \Theta_i}{RT}\right]. \tag{30}$$

Here, A_k is the pre-exponential factor, β_k is the temperature exponent, and E_{a_k} is the activation energy.

A crucial issue with many of the mechanisms published is thermodynamic (in)consistency. Even though most of the mechanisms lead to consistent enthalpy diagrams, many are not consistent regarding the entropy change in the overall reaction due to lack of knowledge of the

transition states of the individual reactions, and therefore of the pre-exponentials in the rate equations. It should be noted that fuel cell modeling strictly requires thermodynamically consistent kinetics, for instance, for modeling the internal fuel reforming in an anode of an SOFC. Lately, optimization procedures enforcing overall thermodynamic consistency have been applied to overcome this problem (Maier *et al.*, 2011b; Mhadeshwar *et al.*, 2003).

The development of a reliable surface reaction mechanism is a complex process (Figure 10) which is usually conducted by establishing models for chemical subsystems and subsequent coupling of these sub-mechanisms. In general, mechanism development starts with a tentative reaction mechanism based on experimental surface science studies, on analogy to gas-phase kinetics and organometallic compounds, and on theoretical studies, increasingly including density functional theory and Monte-Carlo simulations as well as UBI-QEP (Shustorovich and Sellers, 1998) methods. This mechanism should include all possible paths for the formation of the chemical species under consideration in order to be ''elementary-like'' and thus applicable under a wide range of conditions. The idea of the mechanism then needs to be evaluated by an extensive amount of experimentally derived data, which are compared to theoretical predictions based on the mechanism. Here, the simulations of the laboratory reactors require appropriate models for all significant processes in order to evaluate the intrinsic kinetics. Sensitivity analysis leads to the crucial steps in the mechanism, for which refined kinetic experiments and data may be needed. It should be noted that, in general, the reaction

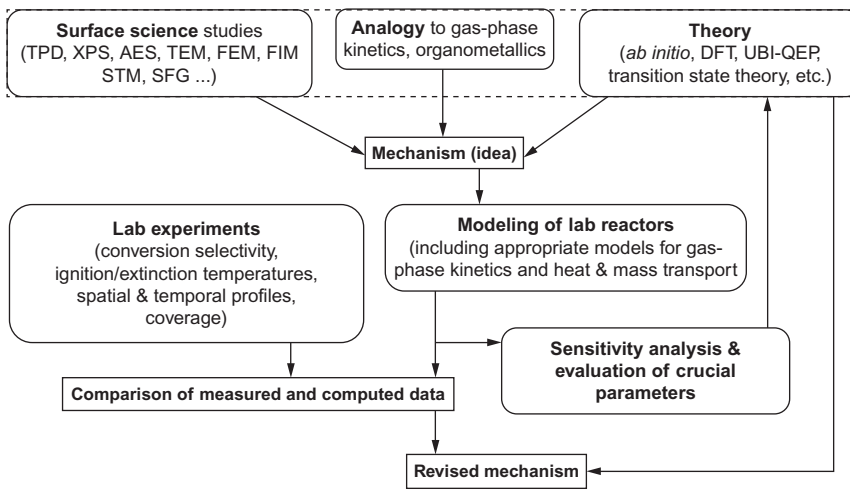

Figure 10 Survey of the methodology of the development of a surface reaction mechanism (Deutschmann, 2008).

kinetics and even the mechanism also depend on many parameters of the catalytic system, such as catalyst particle size and morphology, catalyst pretreatment, catalyst oxidation state, kind and structure of support material, use of additives, and so on.

Here, sensitivity analysis is the computation of the derivatives of the dependent variables (selectivity, conversion, local concentrations, coverages, temperature, etc.) y_i upon the system variables (rate parameters, transport coefficients, etc.):

$$s_{ij} = \frac{\partial y_i}{\partial p_j}. \tag{31}$$

The sensitivity coefficients, s_{ij}, can be computed by several techniques (Campbell, 2001; Coltrin *et al.*, 1991; Deutschmann, 1996).

Especially oxidation and reforming reactions have been modeled extensively by using the MF approach. Since these mechanisms are based on molecular processes, they can be set up to cover all significant macroscopically observed reactions, such as POX and total oxidation, SR and DR, WGS reactions, and pyrolysis. For example, Table 5 shows the reaction steps with the corresponding rate coefficients used for SR of methane over Ni (Maier *et al.*, 2011b). Several of those mechanism, which are relevant for processing different fuels such as methane (Aghalayam *et al.*, 2003; Bui *et al.*, 1997; Deutschmann *et al.*, 1996; Dogwiler *et al.*, 1999; Hickman and Schmidt, 1993b; Veser *et al.*, 1997) and ethane (Donsi *et al.*, 2005; Huff and Schmidt, 1993; Huff *et al.*, 2000; Zerkle *et al.*, 2000) over Pt, and for the formation of hydrogen and synthesis gas over Rh from different hydrocarbons (Hartmann *et al.*, 2010; Hecht *et al.*, 2005; Hickman and Schmidt, 1993b; Schwiedernoch *et al.*, 2003; Thormann *et al.*, 2009), have been developed in the last decade. Adsorption and desorption of radicals are often included in the mechanism. These reactions of intermediately formed species are significant not only for the heterogeneous reaction but also for homogeneous conversion in the surrounding fluid. In most cases, the catalyst acts as sink for radicals produced in the gas phase, and hence radical adsorption slows down or even inhibits gas-phase reaction rates. The interaction between homogeneous and heterogeneous reactions in high-temperature catalysis is still not well-understood; for instance, a recent experimental study has revealed that significant amounts of olefins occur even in the fluid phase of tiny catalytic channels in CPOX of propane (Donazzi *et al.*, 2011).

6.2 Modeling the rate of homogeneous reactions in the gas phase

In many catalytic fuel reformers operated at high temperature, the reactions do not exclusively occur on the catalyst surface but also in the fluid flow. Whenever C_{2+} species are involved in high-temperature reforming,

Table 5 Surface reaction mechanism for steam reforming over Ni following the mean-field approximation, taken from www.detchem.com

	Reaction	A [cm, mol, s]	E_a [kJ/mol]	β [−]
R1	$H_2 + 2Ni(s) \rightarrow 2H(s)$	1.000×10^{-2}	0.0	0.0
R2	$2H(s) \rightarrow 2Ni(s) + H_2$	$2.545 \times 10^{+19}$	81.21	0.0
R3	$O_2 + 2Ni(s) \rightarrow 2O(s)$	1.000×10^{-2}	0.0	0.0
R4	$2O(s) \rightarrow 2Ni(s) + O_2$	$4.283 \times 10^{+23}$	474.95	0.0
R5	$CH_4 + Ni(s) \rightarrow CH_4(s)$	8.000×10^{-3}	0.0	0.0
R6	$CH_4(s) \rightarrow CH_4 + Ni(s)$	$8.705 \times 10^{+15}$	37.55	0.0
R7	$H_2O + Ni(s) \rightarrow H_2O(s)$	1.000×10^{-1}	0.0	0.0
R8	$H_2O(s) \rightarrow H_2O + Ni(s)$	$3.732 \times 10^{+12}$	60.79	0.0
R9	$CO_2 + Ni(s) \rightarrow CO_2(s)$	1.000×10^{-5}	0.0	0.0
R10	$CO_2(s) \rightarrow CO_2 + Ni(s)$	$6.447 \times 10^{+7}$	25.98	0.0
R11	$CO + Ni(s) \rightarrow CO(s)$	5.000×10^{-1}	0.0	0.0
R12	$CO(s) \rightarrow CO + Ni(s)$	$3.563 \times 10^{+11}$	$111.27 - 50\theta_{CO(s)}$	0.0
R13	$CH_4(s) + Ni(s) \rightarrow CH_3(s) + H(s)$	$3.700 \times 10^{+21}$	57.7	0.0
R14	$CH_3(s) + H(s) \rightarrow CH_4(s) + Ni(s)$	$6.034 \times 10^{+21}$	61.58	0.0
R15	$CH_3(s) + Ni(s) \rightarrow CH_2(s) + H(s)$	$3.700 \times 10^{+24}$	100.0	0.0
R16	$CH_2(s) + H(s) \rightarrow CH_3(s) + Ni(s)$	$1.293 \times 10^{+23}$	55.33	0.0
R17	$CH_2(s) + Ni(s) \rightarrow CH(s) + H(s)$	$3.700 \times 10^{+24}$	97.10	0.0
R18	$CH(s) + H(s) \rightarrow CH_2(s) + Ni(s)$	$4.089 \times 10^{+24}$	79.18	0.0
R19	$CH(s) + Ni(s) \rightarrow C(s) + H(s)$	$3.700 \times 10^{+21}$	18.8	0.0
R20	$C(s) + H(s) \rightarrow CH(s) + Ni(s)$	$4.562 \times 10^{+22}$	161.11	0.0
R21	$CH_4(s) + O(s) \rightarrow CH_3(s) + OH(s)$	$1.700 \times 10^{+24}$	88.3	0.0
R22	$CH_3(s) + OH(s) \rightarrow CH_4(s) + O(s)$	$9.876 \times 10^{+22}$	30.37	0.0
R23	$CH_3(s) + O(s) \rightarrow CH_2(s) + OH(s)$	$3.700 \times 10^{+24}$	130.1	0.0
R24	$CH_2(s) + OH(s) \rightarrow CH_3(s) + O(s)$	$4.607 \times 10^{+21}$	23.62	0.0
R25	$CH_2(s) + O(s) \rightarrow CH(s) + OH(s)$	$3.700 \times 10^{+24}$	126.8	0.0
R26	$CH(s) + OH(s) \rightarrow CH_2(s) + O(s)$	$1.457 \times 10^{+23}$	47.07	0.0
R27	$CH(s) + O(s) \rightarrow C(s) + OH(s)$	$3.700 \times 10^{+21}$	48.1	0.0
R28	$C(s) + OH(s) \rightarrow CH(s) + O(s)$	$1.625 \times 10^{+21}$	128.61	0.0
R29	$H(s) + O(s) \rightarrow OH(s) + Ni(s)$	$5.000 \times 10^{+22}$	97.9	0.0
R30	$OH(s) + Ni(s) \rightarrow H(s) + O(s)$	$1.781 \times 10^{+21}$	36.09	0.0
R31	$H(s) + OH(s) \rightarrow H_2O(s) + Ni(s)$	$3.000 \times 10^{+20}$	42.7	0.0
R32	$H_2O(s) + Ni(s) \rightarrow H(s) + OH(s)$	$2.271 \times 10^{+21}$	91.76	0.0
R33	$OH(s) + OH(s) \rightarrow H_2O(s) + O(s)$	$3.000 \times 10^{+21}$	100.0	0.0
R34	$H_2O(s) + O(s) \rightarrow OH(s) + OH(s)$	$6.373 \times 10^{+23}$	210.86	0.0
R35	$C(s) + O(s) \rightarrow CO(s) + Ni(s)$	$5.200 \times 10^{+23}$	148.1	0.0
R36	$CO(s) + Ni(s) \rightarrow C(s) + O(s)$	$1.354 \times 10^{+22}$	$116.12 - 50\theta_{CO(s)}$	−3.0
R37	$CO(s) + O(s) \rightarrow CO_2(s) + Ni(s)$	$2.000 \times 10^{+19}$	$123.6 - 50\theta_{CO(s)}$	0.0

(*continued*)

TABLE 5 (*continued*)

	Reaction	A [cm, mol, s]	E_a [kJ/mol]	β [−]
R38	$CO_2(s)+Ni(s)\rightarrow CO(s)+O(s)$	$4.653\times10^{+23}$	89.32	−1.0
R39	$CO(s)+H(s)\rightarrow HCO(s)+Ni(s)$	$4.019\times10^{+20}$	132.23	−1.0
R40	$HCO(s)+Ni(s)\rightarrow CO(s)+H(s)$	$3.700\times10^{+21}$	$0.0+50\theta_{CO(s)}$	0.0
R41	$HCO(s)+Ni(s)\rightarrow CH(s)+O(s)$	$3.700\times10^{+24}$	95.8	−3.0
R42	$CH(s)+O(s)\rightarrow HCO(s)+Ni(s)$	$4.604\times10^{+20}$	109.97	0.0

significant conversion in the gas phase can occur even at atmospheric pressure. Only in the case of methane reforming, gas-phase reactions can be neglected at pressures up to 10 bars, but not above. Consequently, any simulation of a fuel processor should include an appropriate model for the homogeneous kinetics along with the flow models. Various reliable sets of elementary reactions are available for modeling homogeneous gas-phase reactions, for instance for total oxidation and POX, and pyrolysis of hydrocarbons (Warnatz *et al.*, 1996). In a recent study, Maier *et al.* compared four detailed gas-phase reaction mechanisms concerning their ability to predict homogeneous fuel conversion in CPOX of *iso*-octane and found qualitative but not quantitative agreement between modeling and experimentally determined conversion (Maier *et al.*, 2011a).

In the species mass balance equation, the chemical source term due to homogeneous gas-phase reactions,

$$\sum_{i=1}^{N_g} \nu'_{ik} A_i \rightarrow \sum_{i=1}^{N_g} \nu''_{ik} A_i, \tag{32}$$

is expressed by

$$R_i^{\text{hom}} = M_i \sum_{k=1}^{K_g} \left(\nu''_{ik} - \nu'_{ik}\right) A_k T^{\beta_k} \exp\left[\frac{-E_{a_k}}{RT}\right] \prod_{j=1}^{N_g} c_j^{\nu'_{jk}}. \tag{33}$$

6.3 Coupling of chemistry with mass and heat transport

The chemical processes at the surface can be coupled with the surrounding flow field by boundary conditions for the species-continuity equations at the gas–surface interface (Coltrin *et al.*, 1991; Kee *et al.*, 2003):

$$\vec{n}\left(\vec{j}_i + \rho \vec{v}_{\text{Stef}} Y_i\right) = R_i^{\text{het}} \tag{34}$$

The calculation of the diffusive flux at the gas–surface interface due to adsorption and desorption of reactants and products, respectively,

requires knowledge of the amount of catalytically active surface area as discussed above. The total catalytically active surface area of a metal catalyst is determined experimentally, for example, by chemisorption measurements. The effect of internal mass transfer resistance of the catalyst, dispersed in the usually applied porous washcoat, can be included by an effectiveness factor (Equation (34); Hayes and Kolaczkowski, 1997; Papadias *et al*., 2000). However, more accurate models such as the Dusty Gas Model often need to be applied for an accurate description of the local reaction rate. For more detailed models for transport in porous media, readers are referred to the chapter 6 by Kee *et al*. within this book and to the relevant literature (Deutschmann *et al*., 2001; Kee *et al*., 2003; Keil, 1999, 2000; Mladenov *et al*., 2010).

Even though the implementation of elementary reaction mechanisms in fluid flow models is straightforward, an additional highly nonlinear coupling is introduced into the governing equations leading to considerable computational efforts. The nonlinearity, the very large number (thousands) of chemical species occurring in the reforming of logistic fuels and even in fuel surrogates, and the fact that chemical reactions exhibit a large range of time scales, in particular when radicals are involved, render the solving of those equation systems challenging. In particular for turbulent flows, but sometimes even for laminar flows, the solution of the system is too CPU time-consuming with current numerical algorithms and computer capacities. This calls for the application of reduction algorithms for large reaction mechanisms, for instance by the extraction of the intrinsic low dimensional manifolds of trajectories in chemical space (Maas and Pope, 1992), which can be applied to heterogeneous reactions (Yan and Maas, 2000). Another approach is to use ''as little chemistry as necessary.'' In these so-called adaptive chemistry methods, the construction of the reaction mechanism only includes steps that are relevant for the application studied (Susnow *et al*., 1997).

6.4 Modeling the dynamics of monolithic catalytic reformers

The catalyst-coated monolithic structure given in Figure 3.1 shall serve as an example of modeling a fuel processor (Maier *et al*., 2011a). An efficient approach for modeling such monolithic structures is based on the combination of simulations of a representative number of single channels with the simulation of the temperature profile of the solid structure, treating the latter one as a continuum (Tischer and Deutschmann, 2005; Tischer *et al*., 2001). This approach has been implemented, for instance, in the computer code DETCHEM$^{\text{MONOLITH}}$ (Deutschmann *et al*., 2008), which can be used to model the dynamic behavior of catalytic monoliths. The code combines a transient three-dimensional simulation of a catalytic

monolith with a two-dimensional model of the single-channel flow field, based on the boundary layer approximation. It uses detailed models for homogeneous gas-phase chemistry as well as for heterogeneous surface chemistry and contains a model for the description of pore diffusion in washcoats.

The numerical procedure (Figure 11) is based on the following ideas: The residence time of the reactive gas in the monolith channels is much smaller than the dynamics of the inlet conditions (temperature, mass flow rate, composition) and of the temperature of the solid monolith structure. Particularly in oxidative conversion (POX, ATR), the gas residence time is usually in the order of milliseconds, while the inlet conditions and the temperature of the solid vary in the order of seconds. Under these assumptions, the time scales of the channel flow are decoupled from the dynamics of the temperature of the solid, and the following procedure can be applied: A transient multidimensional heat balance is solved for the monolithic structure, including the thermal insulation and reactor walls, which are treated as a porous continuum. This simulation of the heat balance provides the temperature profiles along the channel walls. At each time step, the reactive flow through a representative number of single channels is simulated, including detailed transport and chemistry models. These single-channel simulations also calculate the heat flux from the fluid flow to the channel wall due to convective and conductive heat transport in the gaseous flow and heat released by chemical reactions.

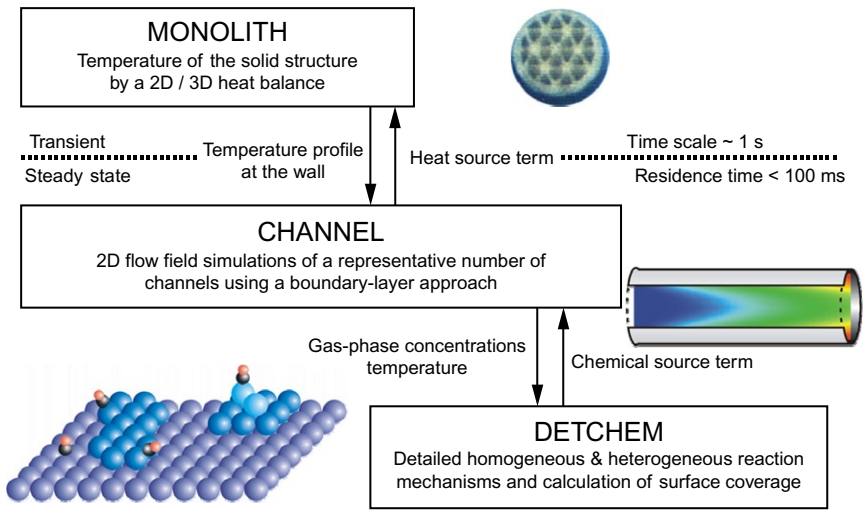

Figure 11 Structure of the code DETCHEM^{MONOLITH} (Deutschmann *et al.*, 2008).

Thus, at each time step, the single-channel simulations provide the source terms for the heat balance of the monolith structure, while the simulation of the heat balance provides the boundary condition (wall temperature) for the single-channel simulations. The inlet conditions may vary at each time step. This very efficient iterative procedure enables a transient simulation of the entire monolith without sacrificing the details of the transport and chemistry models, as long as the prerequisites for the time scales remain valid (Tischer *et al.*, 2001). Furthermore, it is possible to deal with reactors with alternating channel properties, such as flow directions, catalyst materials, and loadings.

6.5 Mathematical optimization of reformer design and operating conditions

In reforming reactors, C/O ratio, steam addition, exhaust recycling, temperature, pressure, and residence time can be used to optimize conversion and selectivity and to avoid formation of harmful by-products. Furthermore, the catalyst loading along the channel can be varied, or even different active components and washcoat structures may be used. Recently, a new mathematical algorithm was developed in order to optimize not only the operating conditions but also the catalyst loading (Minh *et al.*, 2008a,b; von Schwerin *et al.*, 2000). This computational tool was applied to optimize catalytic oxydehydrogenation of ethane at high temperatures and short contact times by Minh *et al.* (2008b). In their study, radical interactions in gas and surface chemistry were shown to play a decisive role in yield increase. These tools may support design and operation of catalytic fuel reformers in the near future.

7. APPLICATIONS OF MODEL-BASED APPROACHES

7.1 Understanding the reaction networks of fuel reforming

Model-based optimization of the reformer design and operating conditions relies on the understanding of the chemical reaction network and the associated kinetics. Two examples will be discussed to illustrate the efforts and the time it takes to reach this kind of understanding: the oxidative reforming of methane and of *iso*-octane serving as fuel surrogates for natural gas and gasoline, respectively. In both cases, the catalyst applied is a rhodium/alumina-coated honeycomb monolith. In both examples, the processes in a single channel of the monolith are analyzed. Even though it is possible to find a set of experimental data using the sufficiently large number of adjustable kinetic parameters of a global

reaction scheme, such as the one given in Section 4.2, little insight can be gained from such a lumped mechanism. Therefore, it is recommended to apply chemical models based on elementary-step reaction mechanisms for understanding the reaction routes.

7.1.1 Reaction networks in the reforming of methane

For reaching a profound understanding of the reaction mechanism of synthesis gas formation from methane by SR, POX, ATR, and DR, the sequence and interaction of the reaction routes have to be analyzed for the combined POX-SR-DR systems, because the conditions in any flow reactor vary along the flow directions, covering a wide range of mixture compositions and leading to quite diverse local reaction rates. There has been a long discussion in literature on the reaction routes in CPOX of methane over Rh and Pt catalysts at short contact times (Deutschmann *et al.*, 2001; Hickman and Schmidt, 1993a,b; Horn *et al.*, 2007, 2006; Schwiedernoch *et al.*, 2003). The crucial point of this discussion was on the formation route of hydrogen. One possible route is direct POX. The other one is an indirect route, in which, at first, total oxidation occurs and subsequently hydrogen is formed by SR of the remaining fuel. Detailed reaction schemes for the CPOX of methane over platinum and rhodium, which also include steps for SR, were published by Schmidt *et al.* (Hickman and Schmidt, 1993b), Vlachos *et al.* (Maestri *et al.*, 2008; Mhadeshwar and Vlachos, 2005, 2007; Mhadeshwar *et al.*, 2003), and Deutschmann *et al.* (Deutschmann *et al.*, 1994, 1996; Quiceno *et al.*, 2006; Schwiedernoch *et al.*, 2003). A unified mechanism covering all aspects of SR and DR, POX and total oxidation, carbon formation, and catalyst oxidation is still under construction. Recently obtained new experimental data for DR (McGuire *et al.*, 2011) call for further adaption of the kinetic schemes available.

Based on a variety of experimental and modeling techniques, a general consensus is now achieved on the reaction routes in CPOX over Rh catalysts: In a quasi two-step process (indirect route), first CH_4 is completely oxidized to CO_2 and steam, as long as oxygen is present close to the catalyst surface, and then the remaining CH_4 is reformed with the steam to synthesis gas (Hannemann *et al.*, 2007; Horn *et al.*, 2010; Schwiedernoch *et al.*, 2003). DR does not play any significant role and the surface acts as a sink for radicals, inhibiting significant gas-phase reactions at pressures below 10 bars (Quiceno *et al.*, 2006). The reaction is mass transport limited, in particular in the total oxidation zone of the reactor, in which the surface reaction rate is very fast in comparison to diffusion of oxygen to the channel wall, which leads to almost zero oxygen concentrations at the gas–catalyst interphase. The decisive proof for this reaction route came from the application of *in situ* techniques to determine spatially resolved species and temperature profiles inside the reactor. The optically accessible catalytic channel

reactor of the Mantzaras group (PSI, Switzerland) was used to resolve the axial and radial profiles in CPOX with exhaust gas recycling of methane at elevated pressure and to compare them with reactor simulations including detailed reaction mechanisms; results are shown in Figure 12 (Schneider *et al.*, 2007, 2006). The Horn group (FHI, Berlin) has recently developed an *in situ* sampling capillary technique for measurements of spatially resolved profiles in reforming catalytic foams up to 1300 °C and 45 bars and also applied this technique to elucidate axial profiles in POX of methane over noble metal catalyst (Horn *et al.*, 2010).

Since natural gas contains higher alkanes and other minor components besides methane, conversion and selectivity can be influenced by these other components. Consequently, conversion of methane in SR of pure methane and in SR of natural gas (North Sea H) differs from each other (Schadel and Deutschmann, 2007; Schadel *et al.*, 2009). Before substantial conversion of methane sets in, most of the heavier hydrocarbons are fully converted.

Another very interesting topic from an external as well as from an internal view point are oxidation and reforming of natural gas over nickel-based catalysts, for which many kinetic studies have been conducted (Mogensen *et al.*, 2011; Rostrup-Nielsen and Hansen, 1993; Wei and Iglesia, 2004; Xu and Froment, 1989a,b). A review on CPOX of methane to synthesis gas, with emphasis on reaction mechanisms over transition metal catalysts, was recently published by Holmen and coworkers (Enger *et al.*, 2008). A hierarchical, multiscale modeling approach recently demonstrated by Chen *et al.* (2011) included a microkinetic model for steam methane reforming on the supported Ni catalyst, including reaction steps of surface carbon formation, segregation, diffusion, and precipitation. The mechanism developed for Ni/alumina catalysts (Maier *et al.*, 2011b) in Table 5 was also successfully applied in numerical simulation of internal SR and DR of

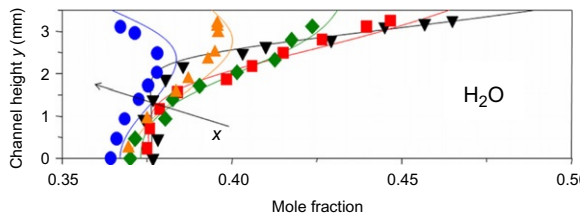

Figure 12 Predicted (lines) and measured (symbols) steam profiles for autothermal reforming of methane over Rh at 6 bars, equivalence ratio of 4, and 38% steam addition, adapted from Schneider *et al.* (2007). The profiles are given at different axial positions of $x = 2$ (black triangle), 5 (red square), 9 (green diamond), 13 (orange triangle), and 17 (blue sphere) cm; the arrow denotes the flow direction (x); catalytic wall at $y = 3.5$ mm, channel centerline at $y = 0$.

methane over Ni/YSZ anodes of SOFCs (Hecht *et al.*, 2005; Janardhanan and Deutschmann, 2006). More details are given in the subsequent chapters of this book.

7.1.2 Reaction networks in the reforming of *iso*-octane

In comparison to the reforming of natural gas, the kinetics of the reforming of higher hydrocarbons is much more challenging, not only due to the fact that the catalytic reaction cycle becomes very complex, but also due to the fact that conversion in the gas phase cannot be neglected any more. In particular, the formation of coke precursors is expected to occur in the gas phase. Several fundamental studies (Hartmann *et al.*, 2011, 2010; Maier *et al.*, 2011a) have recently been conducted to achieve a better understanding of the interactions of surface and gas-phase reactions as well as of mass transport (radial diffusion) in the reforming of liquid hydrocarbons by CPOX. In these studies, *iso*-octane served as model fuel for gasoline. The impact of other gasoline components is discussed above. Again, the process is analyzed in a single monolith channel.

Experimental studies (Hartmann *et al.*, 2009a,b) have revealed the product composition of *iso*-octane in CPOX over a rhodium/alumina-coated honeycomb monolith at a varying C/O ratio. Very high hydrogen and carbon monoxide yields are found at stoichiometric conditions (C/O = 1), while at lean conditions, more total oxidation occurs. At rich conditions (C/O > 1), the formation of by-products such as olefins is observed.

In the modeling approach, the single channel of the monolith at isothermal conditions was numerically simulated, using a two-dimensional parabolic flow field description (Raja *et al.*, 2000). The chemical models need to be able to predict all macrokinetic features from total oxidation via POX, SR, DR, WGS to fuel pyrolysis, and in addition, potential conversion of the fuel in the gas phase should be taken into account. Therefore, the flow field was coupled with elementary-step-based heterogeneous and homogeneous reaction mechanisms (software DETCHEM$^{\text{CHANNEL}}$; Deutschmann *et al.*, 2008; Tischer and Deutschmann, 2005). Since the actual decomposition of adsorbed *iso*-octane over Rh is not known in detail, a simplified approach was proposed (Hartmann *et al.*, 2010): The heterogeneous POX of *i*-octane on rhodium-based catalysts is modeled by a detailed surface reaction mechanism for POX of C_1–C_3 species (Hartmann *et al.*, 2010), consisting of 56 reactions and 17 adsorbed species. This scheme is extended by two additional ''lumped'' reactions for adsorption of *iso*-octane, assuming that *iso*-octane adsorption quickly leads to the species that are explicitly described in the mechanism. For the description of gas-phase kinetics, a reaction mechanism developed by the combustion group at Lawrence Livermore National Laboratory for homogeneous oxidation of *i*-octane

(2,2,4-trimethylpentane) (Curran *et al.*, 2002) was applied; it consists of 7193 irreversible reactions among 857 species.

The numerical simulation, combined with an experimental study, revealed the roles of surface, gas-phase, and radical chemistries in high-temperature oxidative catalytic conversion of *iso*-octane over Rh catalysts. From Figure 13, it can clearly be concluded that the major products (syngas) are produced in the entrance region of the catalyst on the catalytic surface; radial concentration profiles are caused by a mass-transfer limited process. As soon as the oxygen is consumed on the catalytic surface—similar to CPOX of natural gas—hydrogen formation increases due to SR; the major products are formed within few millimeters. At rich conditions (C/O > 1.0), a second process, now in the gas phase, begins in the downstream part, as shown in Figure 14. The number of radicals in the gas phase is sufficiently large to initiate gas-phase pyrolysis of the remaining fuel and formation of coke precursors such as ethylene and propylene.

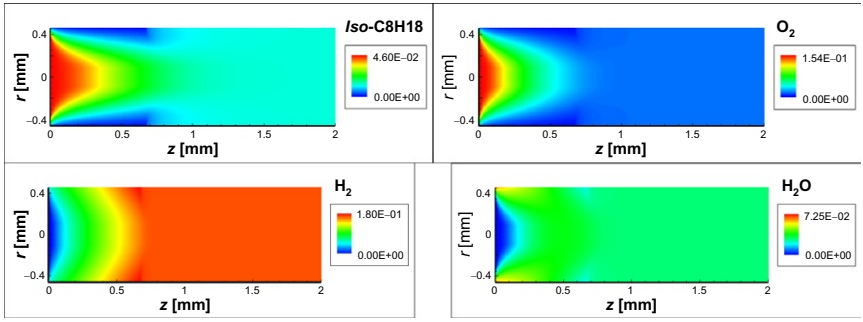

Figure 13 Numerically predicted profiles of molar fractions of reactants and major products in the entrance region of the catalyst at C/O = 1.2 in CPOX of *iso*-octane over a Rh/alumina-coated monolith, taken from Hartmann *et al.* (2010). Flow direction is from left to right.

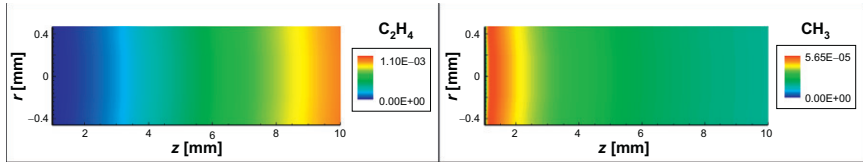

Figure 14 Numerically predicted profiles of molar fractions of ethylene and the CH_3 radical along the entire catalyst at C/O = 1.2 in CPOX of *iso*-octane over a Rh/alumina-coated monolith, taken from Hartmann *et al.* (2010). Flow direction is from left to right.

The Beretta group (Politecnico di Milano) has recently been able to show by a quartz capillary sampling technique that olefins are formed even in the initial catalyst section over a Rh/alumina catalysts in CPOX of propane (Donazzi *et al.*, 2011), which clearly reveals that the application of two-zone model is risky. In these models, it is assumed that, in the first section of the catalyst, only catalytic conversion is significant, and then, further downstream, only gas-phase chemistry needs to be considered.

In the experiment, the downstream part of the catalyst is coked-up; here, the Rh surface cannot act as a sink for radicals. The study also numerically simulated the coverage of the Rh catalyst as a function of the axial coordinate, revealing a sufficient number of unoccupied surface sites at lean (C/O = 0.8) conditions (Figure 15 (left)). At rich conditions (C/O = 1.2; Figure 15 (right)), however, the surface further downstream is completely covered by carbon. This study (Hartmann *et al.*, 2010) also revealed that the applied chemical models—even the most detailed ones available—need further improvement, in particular regarding the formation of minor by-products at rich conditions.

7.2 Predicting and controlling coking in fuel reformers

7.2.1 Catalyst deactivation due to coking

The model discussed above predicts a surface completely covered by carbon, C(s), in the downstream section of the catalyst, $z > 1$ mm. Since the model does not include direct interactions between gas-phase species and carbon on the surface, the gas-phase conversion practically proceeds

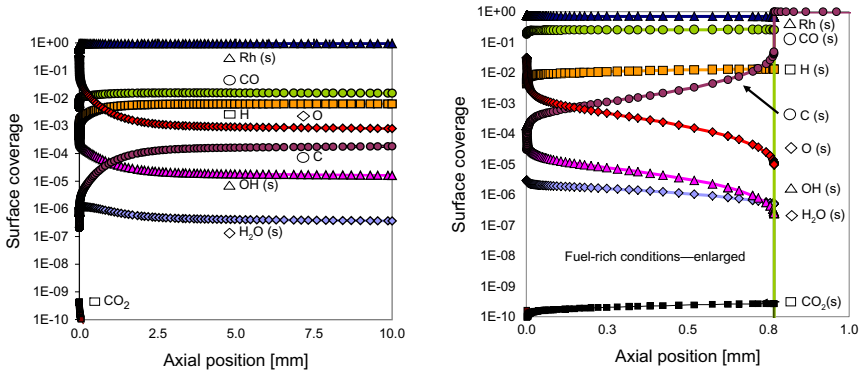

Figure 15 Numerically predicted surface coverage as a function of axial position along the honeycomb catalyst channel in CPOX of *iso*-octane over a Rh/alumina-coated monolith. Conditions: C/O = 0.8, 1359 K (left), C/O = 1.2, 1076 K (right); taken from Hartmann *et al.* (2010).

independently of any direct influence of the catalytic surface, which means radicals are not recombined on the surface for $z > 1$ mm. However, both heterogeneous and homogeneous chemistries are coupled, because the resulting carbonaceous overlayer on the catalyst is a result of the composition of gas phase near the channel wall. The exact position of this C(s) layer is rather sensitive to small variations of several physical parameters such as reactor temperature, catalyst loading, flow rate, and diffusion models. Furthermore, it always occurs in the first third of the catalyst at a given C/O ratio and is very typical for the rich regime, as observed experimentally (Figure 16) (Hartmann, 2009). First studies indicate that the catalyst still shows some activity in that region. A recent AFM study (Essmann, 2011; Essmann *et al.*, 2011) of the initial state of coking in high-temperature reforming led to the conclusion that coke formation indeed starts at the catalyst particle and then spreads over the support. However, the mechanism of coke formation very much depends on the local conditions and temperature. Three different kinetic regimes have recently been observed in high-temperature reforming of hydrocarbons, two initiated by the catalytic particle, and one by deposition from the gas phase at higher temperatures and at a much larger rate (Schädel, 2008).

7.2.2 Quantitative model prediction of formation of coke precursors in the gas phase

The olefins formed in the gas phase have a particularly high potential to form soot particles further downstream of the catalyst, because it will be difficult to cool down the hot product fast enough to avoid any further gas-phase reactions, and therefore, molecular growth of olefins to PAHs will occur. The formed particles are a definite threat for other devices such

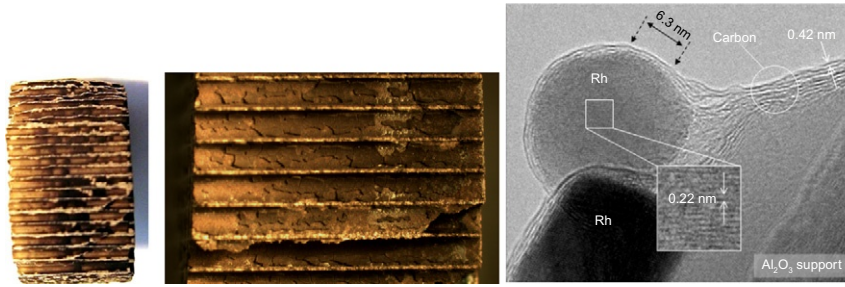

Figure 16 Coke formation on the inner catalytic channel walls and TEM image of carbon-covered Rh particle after the honeycomb was used for several hours in a CPOX reactor operated with *iso*-octane as feed at $C/O > 1.0$. Pictures are taken from Hartmann (2009).

as fuel processing systems and fuel cells, which are located downstream of the CPOX reactor. Adequate measures are required to either avoid operation of the CPOX reactor in a regime where gas-phase reactions are likely to produce precursors of particulate matter, to reduce olefin concentrations with postcatalyst conversion strategies, or to collect the particles formed, for example, by means of the filters.

Gas-phase-initiated coking of the product lines downstream of the catalytic section of the reactors, caused by the olefin precursors formed in the catalytic section, is the topic of a recent study (Kaltschmitt *et al.*, 2011). The product composition of CPOX of *iso*-octane was chosen as the feed composition in a pure gas-phase experiment, in which the product stream was fed into an empty quartz tube heated up to a temperature typical for the catalyst exit temperature of the CPOX reactor, in order to mimic the conditions downstream the catalyst. This homogeneous reactor was also modeled using two different large elementary-step reaction mechanisms. The study concluded that gas-phase reactions among a multitude of species are responsible for coke formation when unconverted fuel leaves the high-temperature oxidation zone in the catalyst. Large amounts of olefinic hydrocarbons are initially formed by thermal cracking, leading to aromatic molecules and further downstream to PAH formation (Figure 17). The presence of gas-phase reactions in the postcatalytic zone decreases the amount of hydrogen produced by methanation and hydrogenation of carbon monoxide and olefins, especially at fuel-rich conditions. Cracking of the remaining fuel increases the concentration of by-products (ethylene, acetylene, and C_3–C_4 olefins) and, as a consequence, also increases the amount of carbon deposits. A conclusion of their study is that the experimentally determined yields (major as well as minor products) in laboratory CPOX reactors may deviate from the local yields at the catalyst exit, because the products cannot usually be quenched fast enough to avoid gaseous postreactions occurring within millimeters beyond the catalyst.

7.3 Impact of the flow rate on reforming efficiency

In Figure 18, the impact of the flow rate on the temperature distribution in the monolithic sections of a short-contact-time reactor for the reforming of *iso*-octane to hydrogen-rich synthesis gas reveals that higher flow rates lead to an increase in temperature and in conversion, and consequently lead to higher hydrogen yields (Maier *et al.*, 2011a). This counter-intuitive increase in fuel conversion with decreasing residence time (increasing flow rate) can be explained by analyzing the ratio of chemical heat release to heat loss in the reactor (Hartmann *et al.*, 2011). Maier *et al.* (2011a) have shown that choosing the right model to account for heat transfer in CPOX reactors helps to understand the impact of the flow rate on conversion

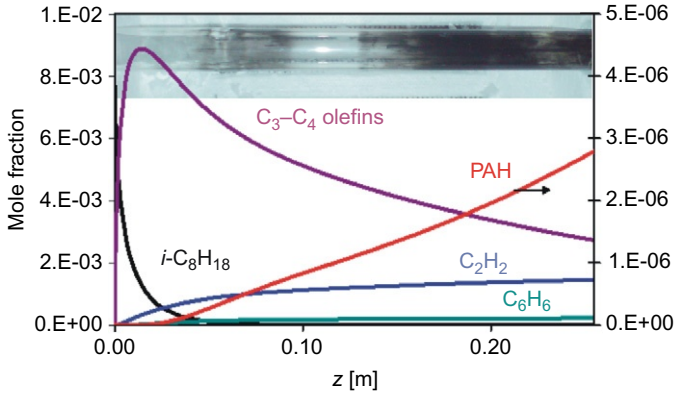

Figure 17 Influence of gas-phase reactions on the catalyst exhaust composition in the postcatalyst zone of a CPOX reformer (Rh/alumina honeycomb) operated with *iso*-octane at rich conditions (C/O = 1.6). The catalyst exhaust composition measured was fed into an empty tube heated by a furnace to a temperature of 1106 K, which was the catalyst exit temperature measured in the CPOX reactor. The figure shows the numerically predicted distribution of carbon precursors along the empty tube, thereby clearly revealing postcatalyst conversion in the downstream gas phase. C_3–C_4 olefins contain 1,2-propadiene, propene, propyne, *n*-butene (1-butene, 2-butene), *iso*-butene, and 1,3-butadiene; PAH contains naphthalene, anthracene, and pyrene. The embedded photo shows the tubular quartz reactor after operation. Taken from Kaltschmitt *et al.* (2011).

and selectivity. An adiabatic single-channel simulation will fail; it is not able to predict even the qualitative behavior, that is, the increase of the catalytic exit temperature with increasing flow rate as shown in Figure 18 (Hartmann *et al.*, 2011). Instead, the entire catalytic monolith with at least several representative channels has to be considered, including heat transport within the solid structure of the monolith and at all monolith boundaries. The increase in temperature with increasing flow rates can be explained by the effect of heat losses. The total amount of heat released by the reaction almost linearly increases with the flow rate, because the fuel is fully converted in the first zone of the catalyst. However, since higher temperature favors the less exothermic POX over the highly exothermic total oxidation, a self-limiting process concerning the temperature increase occurs. Consequently, the temperatures do not increase extraordinarily with increasing flow rate. The total amount of heat loss to the ambience by means of thermal conduction and radiation mainly depends on the temperature of the solid structure, which indeed is higher, but not so much higher as to compensate for the larger heat release effect. In short, the ratio of chemical heat release to thermal heat loss increases with increasing flow

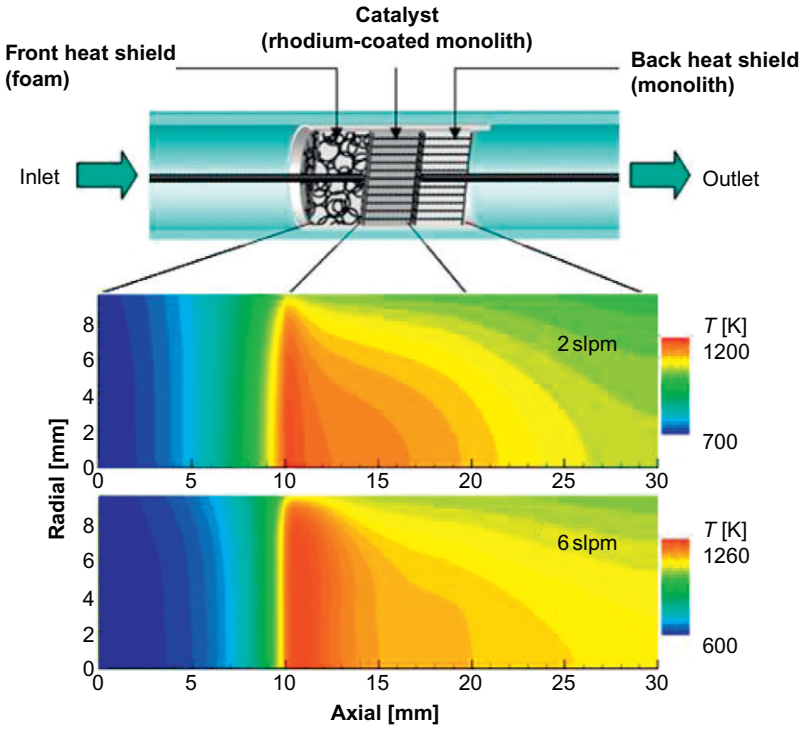

Figure 18 Sketch of the catalyst section of a reformer for logistic fuels with two heat shields (top) and numerically predicted steady-state monolith temperature at C/O = 1.0 and at flow rates of 2 slpm (middle) and 6 slpm (bottom) in CPOX of *iso*-octane over a Rh/alumina-coated honeycomb monolith. The symmetry axis of the monolith is at radial dimension of zero. Taken from Maier *et al.* (2011a).

rate, and therefore, the temperature increases. Higher temperature generally leads to higher hydrogen yields due to thermodynamics. The product composition strongly depends on the flow rate, in particular at higher C/O ratios (Hartmann *et al.*, 2011). The propensity of the formation of coke precursors is also influenced by the flow rate. As shown in Figure 18, the more exterior channels of the monolith exhibit lower temperatures which consequently have an impact on the concentration profiles in the individual channels; not all channels behave essentially alike.

Higher temperatures do not only shift the thermodynamic equilibrium toward hydrogen production, but also increase the reaction rate of the second global reaction step, that is, hydrogen production by SR. The negative temperature gradient in the SR zone is larger for higher flow rates, even though the cooling effect by heat loss of the catalyst to the

ambience is smaller for higher flow rates (Figure 18). However, the heat loss effect clearly overlaps with the flow rate effect. At low flow rates, more exterior channels of the monolith experience much lower temperatures than at high flow rates and, consequently, hydrogen production is reduced. In addition to SR, the exothermic WGS reaction also leads to hydrogen production; this effect is rather small but still has some impact on the final product composition and catalyst outlet temperature (Hartmann *et al.*, 2011). In summary, an understanding of the dependence of hydrogen selectivity on the flow rate can only be achieved by taking mass and heat transfer as well as detailed kinetic schemes (reaction pathways) into account.

7.4 Understanding the dynamics of catalytic monoliths—CPOX of methane

In reformers, a highly dynamic behavior is observed during light-off and shut-down. This transient behavior during light-off of the reaction has been studied in detail for CPOX of methane in a Rh-coated honeycomb reformer. Applying the code DETCHEM^{MONOLITH} described in Section 6, the transient behavior of the temperature of the solid structure of the catalyst and the processes in the single channels can be computed. Figure 19 shows the time-resolved temperature and species profiles in a single channel of a catalytic monolith for POX of methane for the production of synthesis gas and the temperature distribution of the solid structure during light-off (Schwiedernoch *et al.*, 2003).

7.5 Model-based optimization of fuel processor design

In technical systems, overall efficiency is increased by heat integration, which can be realized either directly or indirectly. Figure 20 shows the schematic of a potential technical application, in which the hot exhaust of the SOFC stack at approximately 800 °C is led through the casing of the reformer to improve the heat balance (Goldin *et al.*, 2009). In the case of co-feeding part of the exhaust directly to the fuel/air mixture, one has to be aware of the fact that the oxygen contained in steam and in particular in carbon dioxide may show different reactivity than the oxygen of O_2 (Kaltschmitt *et al.*, 2012).

8. SUMMARY AND CONCLUSIONS

First of all, many items have to be considered when converting the chemical feedstock available in nature such as natural gas, crude oil, coal, and ''regenerative'' sources (biomass) into fuels that fuel cells can

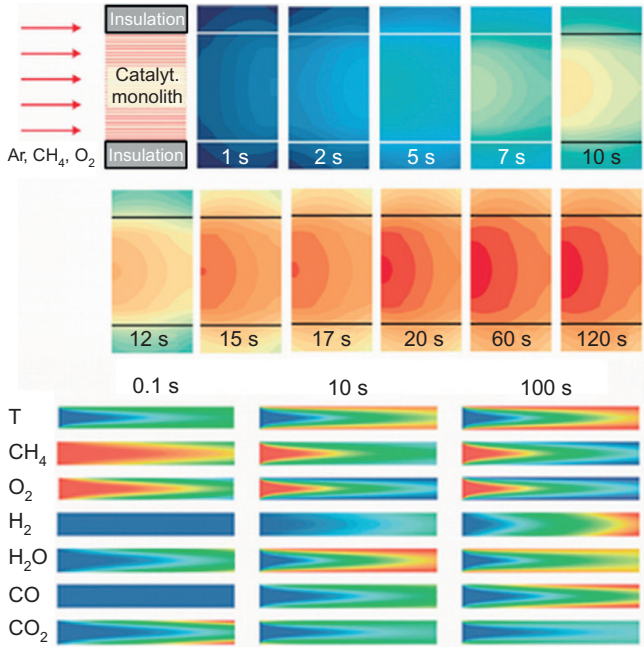

Figure 19 Numerical simulation of the light-off of a Rh/Al_2O_3-coated monolithic honeycomb reactor for partial oxidation of methane to synthesis gas (Schwiedernoch *et al.*, 2003). Top panel: temperature of the solid structure of the catalytic monolith and the thermal insulation (675 K (blue) to 925 K (red)). Lower panel: gas-phase temperature (385–900 K) and species mole fractions (CH_4: 0.043–0.094, O_2: 0–0.055, H_2: 0–0.0412, H_2O: 0–0.058, CO: 0–0.042, CO_2: 0–0.056) in a single channel in the center of the monolith, red = maximum, blue = minimum. The time is set to zero when significant amounts of products can be observed after the reactor was heated up to the ignition temperature of 675 K.

be operated with. Eventually, the fuel cell type and its operating temperature eventually determine the chemical composition of the fuel for the fuel cell. In most cases, hydrogen or hydrogen-rich gases are used as fuel. The amount of other components aside from the hydrogen the cell can take without damage or loss in performance can vary from few ppm in the case of low-temperature PEMFCs to 100% in the case of high-temperature SOFCs. The maximum amount of by-products specified by the fuel cell type under consideration basically determines the amount of final cleaning of the fuel such as removal of CO and hydrocarbons. The original chemical feedstock is usually not directly used in a fuel processor designed for the specific fuel cell application, rather logistically available

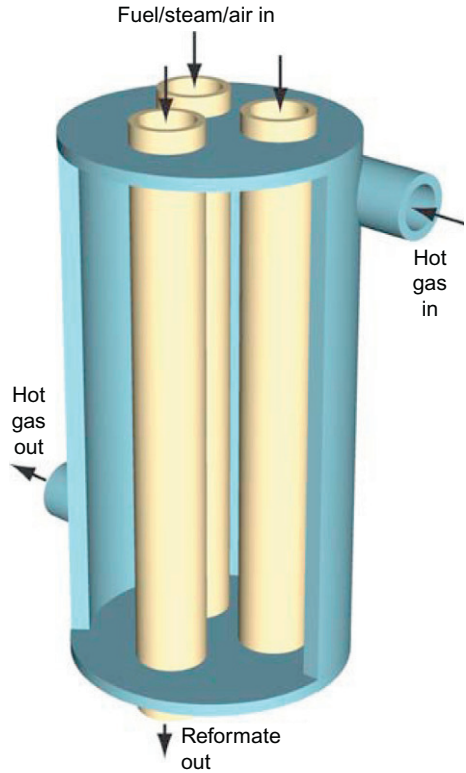

Figure 20 Illustration of a shell-and-tube reformer. Catalytic reforming proceeds within the tubes, with the outer shell flow (exhaust gas recycle) used to assist control of the tube temperatures; taken from Goldin *et al*. (2009).

fuels such as precleaned (desulfurization) natural gas, methanol, gasoline, diesel, kerosene, or biomass-derived fuels such as ethanol and FAME are processed. Alternatively, (pure) hydrogen can directly be used as fuel, which originates as by-product from petrochemical refineries and chemical plants or is produced on-purpose from natural gas and large-scale facilities. The latter one uses SR for converting precleaned natural gas to hydrogen in most cases, although alternate routes such as ATR and POX may attain more attraction in the future.

The way the primary hydrocarbon fuels are processed does not only depend on the fuel available (natural gas, diesel, ...) and the fuel needed for the cell (hydrogen, partially reformed hydrogen, others) but also on the availability of steam and energy, on the way the cell and the reformer can be coupled (e.g., tail-gas recycling), and on the specific application

(stationary/mobile/portable) and the electrical output needed. Consequently, there is plenty of room for process optimization.

Process optimization is very expensive when many parameters and constraints are present. Therefore, mathematical methods are substituting more empirical approaches and trial-and-error methods. Mathematical optimization benefits very much from a detailed understanding of the underlying physical and chemical processes of the reformer devices including the catalyst. Therefore, one of the first tasks in model-based optimization of the design and operating conditions of fuel processors is the understanding of the interactions of chemical reactions and mass and heat transfer in the system. Again, mathematical modeling can tremendously support this understanding.

High-temperature catalysis is the primary chemical technology in fuel processing by SR, partial reforming, and ATR, three routes considered today. In particular, CPOX and ATR allow high-throughput reforming of logistic fuels (natural gas, gasoline, diesel, kerosene, ethanol) in compact devices without the need of external energy. POX of these fuels at millisecond contact times over Rh-based catalysts at around 1000 °C and at optimal fuel/oxygen ratios leads to almost total fuel conversion and hydrogen yields being close to the ones at thermodynamic equilibrium.

Conversion and selectivity, however, strongly depend on the molar C/O ratio of the fuel/oxygen/(steam) mixture. In CPOX, the optimal C/O ratio for hydrogen yield is around the stoichiometric ratio of unity; the production of total oxidation products (H_2O, CO_2) and undesired hydrocarbons (soot precursors such as olefins) are favored at lean ($C/O < 1$) and rich ($C/O > 1$) conditions, respectively. However, depending on the type of fuel, the optimal C/O ratio for achieving the maximum hydrogen yield at a minimum amount of undesired by-products (olefins, acetylene, aromatics) can relatively strong deviate from this optimal C/O ratio. Also, the actual composition of a commercial fuel strongly influences hydrogen yield and product selectivity. Here, the structure of the individual fuel components matters more than their chain length. Therefore, the behavior of real fuels in CPOX reformers is difficult to derive from the behavior of single-component surrogates. In particular, diesel and ethanol-blended fuels exhibit a complex behavior, which cannot be linearly extrapolated from the behavior of their single components. In reforming of ethanol, significant amounts of ethylene and acetaldehyde are produced even at low C/O ratios.

The deactivation of the catalyst and of downstream pipes and devices (e.g., fuel cells) due to coking is one of the challenges in the technical realization of CPOX-based APUs. The coking is initiated by the formation of olefins in the gas phase due to oxidative and—even more important—pyrolytic processes; exceptions are methane (no coking at relevant pressure) and ethanol (surface processes seem to matter as well).

As said, modeling and simulation can support the understanding of the interaction of mass and heat transfer with heterogeneous and homogeneous chemical reactions in the reformer. The dependence of product composition on C/O ratio, temperature, and flow rate as well as the occurrence of coke precursors can be explained by modeling work, at least qualitatively. The catalytic conversion is usually controlled by mass transfer (external diffusion). Most reformers operated with fuels that contain aliphatic and aromatic hydrocarbons with two and more carbon atoms exhibit a coupling between catalytic and homogeneous (gas-phase) conversion via adsorbed and desorbed intermediates and radicals. Detailed catalytic reaction mechanisms are only available for natural gas and single-component liquid fuel surrogates such as *iso*-octane and only over rhodium-based catalysts. The extrapolation of the behavior of reformers operated with surrogates (laboratory scale) to the behavior of reformers operated with complex logistic fuels has to be conducted with care. However, studies using surrogates can indeed lead to useful information for the design of reformers and the optimization of operational conditions to maximize hydrogen yield and minimize by-product formation as discussed in this chapter.

ACKNOWLEDGMENTS

The work presented includes studies of former and current PhD students and postdocs in our group at the Karlsruhe Institute of Technology; in particular, we would like to express our appreciation to L. Maier, S. Tischer, R. Schwiedernoch, B. Schädel, M. Hartmann, N. Hebben, C. Diehm, and C. Eßmann and thanks to R. Klinkig for editorial assistance. Financial support by the German Research Foundation (DFG) and many industrial partners is gratefully acknowledged.

REFERENCES

Aghalayam, P., Park, Y. K., Fernandes, N., Papavassiliou, V., Mhadeshwar, A. B. and Vlachos, D. G., *J. Catal.* **213,** 23–38 (2003).

Akdim, O., Cai, W. J., Fierro, V., Provendier, H., Van Veen, A., Shen, W. J. and Mirodatos, C., *Top. Catal.* **51,** 22–38 (2008).

Avgouropoulos, G. and Ioannides, T., *Appl. Catal. Environ.* **67,** 1–11 (2006).

Bion, N., Epron, F., Moreno, M., Marino, F. and Duprez, D., *Top. Catal.* **51,** 76–88 (2008).

Bird, R. B., Stewart, W. E. and Lightfoot, E. N., ''Transport Phenomena''. 2nd ed. John Wiley & Sons, Inc., New York (2001).

Birot, A., Epron, F., Descorme, C. and Duprez, D., *Appl. Catal. Environ.* **79,** 17–25 (2008).

Boll, W., Tischer, S. and Deutschmann, O., *Ind. Eng. Chem. Res.* **49,** 10303–10310 (2010).

Borup, R. L., Inbody, M. A., Semelsberger, T. A., Tafoya, J. I. and Guidry, D. R., *Catal. Today* **99,** 263–270 (2005).

Bui, P.-A., Vlachos, D. G. and Westmoreland, P. R., *Surf. Sci.* **386,** L1029–L1034 (1997).

Campbell, C. T., *J. Catal.* **204,** 520–524 (2001).

Cavallaro, S., *Energy Fuel* **14,** 1195–1199 (2000).
Cavallaro, S., Chiodo, V., Freni, S., Mondello, N. and Frusteri, F., *Appl. Catal. Gen.* **249,** 119–128 (2003a).
Cavallaro, S., Chiodo, V., Vita, A. and Freni, S., *J. Power Sources* **123,** 10–16 (2003b).
CETENA S.p.A. Project MC WAP. http://www.mc-wap.cetena.it.
Chen, D., Lodeng, R., Svendsen, H. and Holmen, A., *Ind. Eng. Chem. Res.* **50,** 2600–2612 (2011).
Chunshan, S., *Catal. Today* **86,** 211–263 (2003).
Coltrin, M. E., Kee, R. J., and Rupley, F. M. (1991). SURFACE CHEMKIN (Version 4.0): A Fortran Package for Analyzing Heterogeneous Chemical Kinetics at a Solid-Surface—Gas-Phase Interface, SAND91-8003B. Sandia National Laboratories.
Costa, L. O. O., Vasconcelos, S. M. R., Pinto, A. L., Silva, A. M., Mattos, L. V., Noronha, F. B. and Borges, L. E. P., *J. Mater. Sci.* **43,** 440–449 (2008).
Courty, P., Chaumette, P., Raimbault, C. and Travers, P., *Rev. Inst. Fr. Petr.* **45,** 561–578 (1990).
Curran, H. J., Gaffuri, P., Pitz, W. J. and Westbrook, C. K., *Combust. Flame* **129,** 253–280 (2002).
Dagle, R. A., Platon, A., Palo, D. R., Datye, A. K., Vohs, J. M. and Wang, Y., *Appl. Catal. Gen.* **342,** 63–68 (2008).
de Lima, S. M., Colman, R. C., Jacobs, G., Davis, B. H., Souza, K. R., de Lima, A. F. F., Appel, L. G., Mattos, L. V. and Noronha, F. B., *Catal. Today* **146,** 110–123 (2009).
Deluga, G. A., Salge, J. R., Schmidt, L. D. and Verykios, X. E., *Science* **303,** 993–997 (2004).
Deutschmann, O. (1996). Modellierung von Reaktionen an Oberflächen und deren Kopplung mit chemisch reagierenden Strömungen. IWR, Universität Heidelberg, Heidelberg, p. 133.
Deutschmann, O., Computational fluid dynamics simulation of catalytic reactors: Chapter 6.6. *in* ''Handbook of Heterogeneous Catalysis'' (G. Ertl, K. Knözinger, F. Schüth and J. Weitkamp, Eds.), 2nd ed. pp. 1811–1828. Wiley-VCH, Weinheim (2008).
Deutschmann, O., (Ed.) ''Modeling and Simulation of Heterogeneous Catalytic Reactions: From the Molecular Process to the Technical System''. Wiley-VCH, Weinheim (2011).
Deutschmann, O. and Schmidt, L. D., *AIChE J.* **44,** 2465–2477 (1998).
Deutschmann, O., Behrendt, F. and Warnatz, J., *Catal. Today* **21,** 461–470 (1994).
Deutschmann, O., Schmidt, R., Behrendt, F. and Warnatz, J., *Proc. Combust. Inst.* **26,** 1747–1754 (1996).
Deutschmann, O., Schwiedernoch, R., Maier, L. I. and Chatterjee, D., *Stud. Surf. Sci. Catal.* **136,** 251–258 (2001).
Deutschmann, O., Tischer, S., Kleditzsch, S., Janardhanan, V. M., Correa, C., Chatterjee, D., Mladenov, N., and Minh, H. D. (2008). DETCHEM^{TM} software package, 2.2 ed. DETCHEM^{TM} software package, www.detchem.com.
Diehm, C. (2010). Katalytische Partialoxidation von ethanolhaltigen Kraftstoffen an Rhodium, Diploma thesis, Fakultät für Chemie und Biowissenschaften, Karlsruher Institut für Technologie (KIT).
Dissanayake, D., Kharas, K. C. C., Lunsford, J. H. and Rosynek, M. P., *J. Catal.* **139,** 652–663 (1993).
Dogwiler, U., Benz, P. and Mantzaras, J., *Combust. Flame* **116,** 243 (1999).
Donazzi, A., Livio, D., Maestri, M., Beretta, A., Groppi, G., Tronconi, E. and Forzatti, P., *Angew. Chem. Int. Ed.* **50,** 3943–3946 (2011).
Donsi, F., Williams, K. A. and Schmidt, L. D., *Ind. Eng. Chem. Res.* **44,** 3453–3470 (2005).
Duisberg, M., Lopez, M., Seitz, K. and Sextl, G., Fuel cells. *in* ''Handbook of Fuels'' (B. Elvers, Ed.), Wiley-VCH, Weinheim (2008).
e4ships. Project SchIBZ. http://www.e4ships.de/project-schibz.html.
Enger, B. C., Lodeng, R. and Holmen, A., *Appl. Catal. A Gen.* **346,** 1–27 (2008).
Essmann, C. (2011). Untersuchung der Verkokung von Rhodiumkatalysatoren während der Wasserdampfreformierung von Erdgas. Doctoral thesis, Fakultät für Chemie und Biowissenschaften, Karlsruhe Institute of Technology.

Essmann, C., Weis, F., Seipenbusch, M., Schimmel, T. and Deutschman, O., *Z. Phys. Chem.* **225,** 1207–1224 (2011).
Fatsikostas, A. N., Kondarides, D. I. and Verykios, X. E., *Catal. Today* **75,** 145–155 (2002).
Fierro, V., Klouz, V., Akdim, O. and Mirodatos, C., *Catal. Today* **75,** 141–144 (2002).
Fierro, V., Akdim, O. and Mirodatos, C., *Green Chem.* **5,** 20–24 (2003).
Fierro, V., Akdim, O., Provendier, H. and Mirodatos, C., *J. Power Sources* **145,** 659–666 (2005).
Fishtik, I., Alexander, A., Datta, R. and Geana, D., *Int. J. Hydrogen Energy* **25,** 31–45 (2000).
Fontaine, J. (2011). Air independent power and energy sources for autonomous undersea vehicles. Fuel Cell Seminar & Exposition, Orlando, FL.
Ghenciu, A. F., *Curr. Opin. Solid State Mater. Sci.* **6,** 389–399 (2002).
Goldin, G., Zhu, H., Katte, K., Dean, A., Braun, R., Kee, R., Zhang, D., Maier, L. and Deutschmann, O., *ECS Trans.* **25,** 1253–1262 (2009).
Gupta, M., Smith, M. L. and Spivey, J. J., *ACS Catal.* **1,** 641–656 (2011).
Hannemann, S., Grunwaldt, J. D., van Vegten, N., Baiker, A., Boye, P. and Schroer, C. G., *Catal. Today* **126,** 54–63 (2007).
Hartmann, M. (2009). Erzeugung von Wasserstoff mittels katalytischer Partialoxidation höherer Kohlenwasserstoffe an Rhodium. Doctoral thesis, Fakultät für Chemie und Biowissenschaften, Universität Karlsruhe (TH).
Hartmann, M., Kaltschmitt, T. and Deutschmann, O., *Catal. Today* **147,** S204–S209 (2009a).
Hartmann, M., Lichtenberg, S., Hebben, N., Zhang, D. and Deutschmann, O., *Chem. Ing. Tech.* **81,** 909–919 (2009b).
Hartmann, M., Maier, L., Minh, H. D. and Deutschmann, O., *Combust. Flame* **157,** 1771–1782 (2010).
Hartmann, M., Maier, L. and Deutschmann, O., *Appl. Catal. A Gen.* **391,** 144–152 (2011).
Hayes, R. E. and Kolaczkowski, S. T., ''Introduction to Catalytic Combustion''. Gordon and Breach Science Publishers, Amsterdam (1997).
Hebben, N., Diehm, C. and Deutschmann, O., *Appl. Catal. A Gen.* **388,** 225–231 (2010).
Hecht, E. S., Gupta, G. K., Zhu, H. Y., Dean, A. M., Kee, R. J., Maier, L. and Deutschmann, O., *Appl. Catal. A Gen.* **295,** 40–51 (2005).
Hennessy, D. (2011). Solid oxide fuel cell development at Delphi. Fuel Cell Seminar & Exposition, Orlando, FL.
Hernandeza, S., Solarino, L., Orsello, G., Russo, N., Fino, D., Saracco, G. and Specchia, V., *Int. J. Hydrogen Energy* **33,** 3209–3214 (2008).
Hickman, D. A. and Schmidt, L. D., *J. Catal.* **138,** 267–282 (1992).
Hickman, D. A. and Schmidt, L. D., *Science* **259,** 343–346 (1993a).
Hickman, D. A. and Schmidt, L. D., *AIChE J.* **39,** 1164–1177 (1993b).
Hohn, K. L. and Lin, Y.-C., *ChemSusChem* **2,** 927–940 (2009).
Horn, R., Williams, K. A., Degenstein, N. J. and Schmidt, L. D., *J. Catal.* **242,** 92–102 (2006).
Horn, R., Williams, K. A., Degenstein, N. J., Bitsch-Larsen, A., Nogare, D. D., Tupy, S. A. and Schmidt, L. D., *J. Catal.* **249,** 380–393 (2007).
Horn, R., Korup, O., Geske, M., Zavyalova, U., Oprea, I. and Schlogl, R., *Rev. Sci. Instrum.* **81,** 6 (2010).
Huff, M. and Schmidt, L. D., *J. Phys. Chem.* **97,** 11815–11822 (1993).
Huff, M. C., Androulakis, I. P., Sinfelt, J. H. and Reyes, S. C., *J. Catal.* **191,** 46–54 (2000).
Janardhanan, V. M. and Deutschman, O., Computational fluid dynamics of catalytic reactors. *in* ''Modeling and Simulation of Heterogeneous Catalytic Reactions: From the Molecular Process to the Technical System'' (O. Deutschman, Ed.), pp. 251–282. Wiley-VCH, Weinheim (2011).
Janardhanan, V. M. and Deutschmann, O., *J. Power Sources* **162,** 1192–1202 (2006).
Kaltschmitt, T., Maier, L., Hartmann, M., Hauck, C. and Deutschmann, O., *Proc. Combust. Inst.* **33,** 3177–3183 (2011).

Kaltschmitt, T., Diehm, C., and Deutschmann, O. (2012). *Ind. Eng. Chem. Res* dx.doi.org/10.1021/ie201712d.
Kang, I., Carstensen, H. H. and Dean, A. M., *Mater. Sci. Forum* **638–642,** 1118–1124 (2010) Thermec 2009.
Kang, I. Y., Carstensen, H. H. and Dean, A. M., *J. Power Sources* **196,** 2020–2026 (2011).
Kee, R. J., Coltrin, M. E. and Glarborg, P., ''Chemically Reacting Flow''. Wiley-Interscience, New York (2003).
Keil, F., ''Diffusion und Chemische Reaktionen in der Gas-Feststoff-Katalyse''. Springer-Verlag, Berlin (1999).
Keil, F. J., *Catal. Today* **53,** 245–258 (2000).
Kirillov, V., Meshcheryakov, V., Sobyanin, V., Belyaev, V., Amosov, Y., Kuzin, N. and Bobrin, A., *Theor. Found. Chem. Eng.* **42,** 1–11 (2008).
Kleiber-Viglione, M., *Power Eng.* **115,** 66 (2011).
Knight, A. R. and Verma, A., *Product R&D* **15,** 59–63 (1976).
Kolb, G., ''Fuel Processing for Fuel Cells''. Wiley-VCH, Weinheim (2008).
Krummenacher, J. J. and Schmidt, L. D., *J. Catal.* **222,** 429–438 (2004).
Krummenacher, J. J., West, K. N. and Schmidt, L. D., *J. Catal.* **215,** 332–343 (2003).
Laosiripojana, N. and Assabumrungrat, S., *Appl. Catal. Environ.* **66,** 29–39 (2006).
Liguras, D. K., Kondarides, D. I. and Verykios, X. E., *Appl. Catal. Environ.* **43,** 345–354 (2003).
Liguras, D. K., Goundani, K. and Verykios, X. E., *J. Power Sources* **130,** 30–37 (2004).
Liu, X. M., Lu, G. Q., Yan, Z. F. and Beltramini, J., *Ind. Eng. Chem. Res.* **42,** 6518–6530 (2003).
Liu, S., Zhang, K., Fang, L. N. and Li, Y. D., *Energy Fuel* **22,** 1365–1370 (2008).
Maas, U. and Pope, S., *Combust. Flame* **88,** 239–264 (1992).
Maestri, M., Vlachos, D. G., Beretta, A., Groppi, G. and Tronconi, E., *J. Catal.* **259,** 211–222 (2008).
Maier, L., Hartmann, M., Tischer, S. and Deutschmann, O., *Combust. Flame* **158,** 796–808 (2011a).
Maier, L., Schädel, B., Herrera Delgado, K., Tischer, S. and Deutschmann, O., *Top. Catal.* **54,** 845–858 (2011b).
McGuire, N. E., Sullivan, N. P., Deutschmann, O., Zhu, H. Y. and Kee, R. J., *Appl. Catal. A Gen.* **394,** 257–265 (2011).
Mhadeshwar, A. B. and Vlachos, D. G., *J. Phys. Chem. B* **109,** 16819–16835 (2005).
Mhadeshwar, A. B. and Vlachos, D. G., *Ind. Eng. Chem. Res.* **46,** 5310–5324 (2007).
Mhadeshwar, A. B., Wang, H. and Vlachos, D. G., *J. Phys. Chem. B* **107,** 12721–12733 (2003).
Minh, H. D., Bock, H. G., Tischer, S. and Deutschmann, O., Fast solution for large-scale 2-D convection-diffusion, reacting flows. *in* Iccsa 2008 Proceedings of the International Conference on Computational Science and Its Applications, Part 1, Vol. 5072, pp. 1121–1130. Springer-Verlag, Berlin (2008).
Minh, H. D., Bock, H. G., Tischer, S. and Deutschmann, O., *AIChE J.* **54,** 2432–2440 (2008b).
Mintz, M. M., Vyas, A. R. D., Wang, M. Q., Stodolsky, F., Cuenca, R. M. and Gaines, L. L., *Energy Air Qual. Fuels* **2000,** 100–105 (2000).
Mladenov, N., Koop, J., Tischer, S. and Deutschmann, O., *Chem. Eng. Sci.* **65,** 812–826 (2010).
Mogensen, D., Grunwaldt, J. D., Hendriksen, P. V., Dam-Johansen, K. and Nielsen, J. U., *J. Power Sources* **196,** 25–38 (2011).
Muradov, N., *J. Power Sources* **118,** 320–324 (2003).
Muradov, N., Ramasamy, K., Linkous, C., Huang, C. P., Adebiyi, I., Smith, F., T-Raissi, A. and Stevens, J., *Fuel* **89,** 1221–1229 (2010).
Ni, M., Leung, D. Y. C. and Leung, M. K. H., *Int. J. Hydrogen Energy* **32,** 3238–3247 (2007).
Nilsson, M., Karatzas, X., Lindstrom, B. and Pettersson, L. J., *Chem. Eng. J.* **142,** 309–317 (2008).

Ochoa-Fernandez, E., Rusten, H. K., Jakobsen, H. A., Ronning, M., Holmen, A. and Chen, D., *Catal. Today* **106,** 41–46 (2005).
O'Connor, R. P., Klein, E. J. and Schmidt, L. D., *Catal. Lett.* **70,** 99–107 (2000).
Oetjen, H. F., Schmidt, V. M., Stimming, U. and Trila, F., *J. Electrochem. Soc.* **143,** 3838–3842 (1996).
Oh, S. H. and Sinkevitch, R. M., *J. Catal.* **142,** 254–262 (1993).
Papadias, D., Edsberg, L. and Björnbom, P. H., *Catal. Today* **60,** 11–20 (2000).
Park, E. D., Lee, D. and Lee, H. C., *Catal. Today* **139,** 280–290 (2009).
Patankar, S. V., ''Numerical Heat Transfer and Fluid Flow''. McGraw-Hill, New York (1980).
Phan, X. K., Bakhtiary-Davijany, H., Myrstad, R., Pfeifer, P., Venvik, H. J. and Holmen, A., *Appl. Catal. Gen.* **405,** 1–7 (2011).
Quiceno, R., Perez-Ramirez, J., Warnatz, J. and Deutschmann, O., *Appl. Catal. A Gen.* **303,** 166–176 (2006).
Raja, L. L., Kee, R. J., Deutschmann, O., Warnatz, J. and Schmidt, L. D., *Catal. Today* **59,** 47–60 (2000).
Ratnasamy, C. and Wagner, J. P., *Catal. Rev. Sci. Eng.* **51,** 325–440 (2009).
Rechberger, J. (2011). First operation experience with AVL SOFC systems. Fuel Cell Seminar & Exposition, Orlando, FL.
Roh, H. S., Wang, Y. and King, D. L., *Top. Catal.* **49,** 32–37 (2008).
Rostrup-Nielsen, J. R., Catalytic steam reforming. *in* ''Catalysis Science and Technology'' (J. R. Anderson and M. Boudart, Eds.Vol 5, pp. 1–117. Springer-Verlag, New York (1984).
Rostrup-Nielsen, J. R. and Hansen, J.-H. B., *J. Catal.* **144,** 38–49 (1993).
Rowe, T. and Karl, F. (2011). Market launch of BlueGen: Essential experience from real-world field trials. Fuel Cell Seminar & Exposition, Orlando, FL.
Ruettinger, W., Liu, X. S. and Farrauto, R. J., *Appl. Catal. Environ.* **65,** 135–141 (2006).
Salge, J. R., Deluga, G. A. and Schmidt, L. D., *J. Catal.* **235,** 69–78 (2005).
Sandstede, G., *Bunsen-Magazin* **2,** 66–69 (2000).
Sato, K., Kawano, K., Ito, A., Takita, Y. and Nagaoka, K., *ChemSusChem* **3,** 1364–1366 (2010).
Schädel, B. (2008). Wasserdampfreformierung von Erdgas mit Rhodiumkatalysatoren: Aktivität und Deaktivierung. Doctoral thesis, Department of Chemistry and Biosciences, University of Karlsruhe, Karlsruhe.
Schadel, B. T. and Deutschmann, O., Steam reforming of natural gas on noble-metal based catalysts: Predictive modeling. (F. B. Noronha, M. Schmal and E. F. SousaAguiar, Eds.), Natural Gas Conversion VIII. Proceedings of the 8th Natural Gas Conversion Symposium, pp. 207–212. (2007).
Schadel, B. T., Duisberg, M. and Deutschmann, O., *Catal. Today* **142,** 42–51 (2009).
Schneider, A., Mantzaras, J. and Jansohn, P., *Chem. Eng. Sci.* **61,** 4634–4649 (2006).
Schneider, A., Mantzaras, J., Bombach, R., Schenker, S., Tylli, N. and Jansohn, P., *Proc. Combust. Inst.* **31,** 1973–1981 (2007).
Schwiedernoch, R., Tischer, S., Correa, C. and Deutschmann, O., *Chem. Eng. Sci.* **58,** 633–642 (2003).
Senanayake, S. D., Stacchiola, D., Liu, P., Mullins, C. B., Hrbek, J. and Rodriguez, J. A., *J. Phys. Chem. C* **113,** 19536–19544 (2009).
Shekhawat, D., Gardner, T. H., Berry, D. A., Salazar, M., Haynes, D. J. and Spivey, J. J., *Appl. Catal. A Gen.* **311,** 8–16 (2006).
Shekhawat, D., Berry, D. A., Haynes, D. J. and Spivey, J. J., *Fuel* **88,** 817–825 (2009).
Shustorovich, E. and Sellers, H., *Surf. Sci. Rep.* **31,** 1–119 (1998).
Silva, A. M., Costa, L. O. O., Barandas, A., Borges, L. E. P., Mattos, L. V. and Noronha, F. B., *Catal. Today* **133,** 755–761 (2008a).

Silva, A. M., De Farias, A. M. D., Costa, L. O. O., Barandas, A., Mattos, L. V., Fraga, M. A. and Noronha, F. B., *Appl. Catal. A Gen.* **334,** 179–186 (2008b).
Simon, M. (2011). DOE Recovery Act Projects to enable fuel cell market transformation. Fuel Cell Seminar & Exposition, Orlando, FL.
Spivey, J. J. and Egbebi, A., *Chem. Soc. Rev.* **36,** 1514–1528 (2007).
Subramanian, R., Panuccio, G. J., Krummenacher, J. J., Lee, I. C. and Schmidt, L. D., *Chem. Eng. Sci.* **59,** 5501–5507 (2004).
Susnow, R. G., Dean, A. M., Green, W. H., Peczak, P. and Broadbelt, L., *J. Phys. Chem. A* **101,** 3731–3740 (1997).
Takahashi, K., Kobayashi, H. and Takezawa, N., *Chem. Lett.* 759–762 (1985).
Takenaka, S., Shimizu, T. and Otsuka, K., *Int. J. Hydrogen Energy* **29,** 1065–1073 (2004).
Thormann, J., Pfeifer, P., Kunz, U. and Schubert, K., *Int. J. Chem. React. Eng.* **6,** 1–18 (2008a).
Thormann, J., Pfeifer, P., Schubert, K. and Kunz, U., *Chem. Eng. J.* **135,** S74–S81 (2008b).
Thormann, J., Maier, L., Pfeifer, P., Kunz, U., Deutschmann, O. and Schubert, K., *Int. J. Hydrogen Energy* **34,** 5108–5120 (2009).
Tischer, S. and Deutschmann, O., *Catal. Today* **105,** 407–413 (2005).
Tischer, S., Correa, C. and Deutschmann, O., *Catal. Today* **69,** 57–62 (2001).
Trimm, D. L., *Catal. Today* **37,** 233–238 (1997).
van Rheinberg, O., Lucka, K. and Kohne, H., *J. Power Sources* **196,** 8983–8993 (2011).
Veser, G., Frauhammer, J., Schmidt, L. D. and Eigenberger, G., *Stud. Surf. Sci. Catal.* **109,** 273–284 (1997).
Vesselli, E., Comelli, G., Rosei, R., Freni, S., Frusteri, F. and Cavallaro, S., *Appl. Catal. A Gen.* **281,** 139–147 (2005).
Villano, S. M., Hoffmann, J., Carstensen, H. H. and Dean, A. M., *J. Phys. Chem. A* **114,** 6502–6514 (2010).
von Schwerin, M., Deutschmann, O. and Schulz, V., *Comput. Chem. Eng.* **24,** 89–97 (2000).
Wanat, E. C., Venkataraman, K. and Schmidt, L. D., *Appl. Catal. A Gen.* **276,** 155–162 (2004).
Wanat, E. C., Suman, B. and Schmidt, L. D., *J. Catal.* **235,** 18–27 (2005).
Warnatz, J., Dibble, R. W. and Maas, U., ''Combustion, Physical and Chemical Fundamentals, Modeling and Simulation, Experiments, Pollutant Formation''. Springer-Verlag, New York (1996).
Wei, J. M. and Iglesia, E., *J. Catal.* **224,** 370–383 (2004).
Wendt, H., *J. Appl. Electrochem.* **35,** 1277–1282 (2005).
Windmann, J., Braun, J., Zacke, P., Tischer, S., Deutschmann, O., and Warnatz, J. (2003). Impact of the inlet flow distribution on the light-off behavior of a 3-way catalytic converter. SAE Technical Paper 2003-01-0937.
Xu, J. G. and Froment, G. F., *AIChE J.* **35,** 97–103 (1989a).
Xu, J. G. and Froment, G. F., *AIChE J.* **35,** 88–96 (1989b).
Yan, X. and Maas, U., *Proc. Combust. Inst.* **28,** 1615–1621 (2000).
Zane, F., Trevisan, V., Pinna, F., Signoretto, M. and Menegazzo, F., *Appl. Catal. Environ.* **89,** 303–308 (2009).
Zerkle, D. K., Allendorf, M. D., Wolf, M. and Deutschmann, O., *J. Catal.* **196,** 18–39 (2000).